Results & Discussion

2. RESULTS AND DISCUSSION

The corrosion of metallic surfaces in acidic solutions causes a considerable cost. In order to reduce the corrosion of metals, several techniques have been applied. The use of corrosion inhibitors is one of the most practical methods for protection against corrosion in acidic media. Corrosion inhibitors which reduce corrosion on metallic surfaces can be divided into four kinds: (i) inorganic inhibitors, (ii) organic inhibitors, (iii) surfactant inhibitors, and (iv) mixed material inhibitors. Surfactant corrosion inhibitors have many advantages such as high inhibition efficiency, low price, low toxicity and easy production. Surfactants are molecules composed of a polar hydrophilic group, the "head", attached to a nonpolar hydrophobic group, the "tail". Generally, in aqueous solution the inhibitory action of surfactant molecules may also be due to physical (electrostatic) adsorption or chemisorption onto the metallic surface, depending on the charge of the solid surface and the free energy change of transferring a hydrocarbon chain from water to the solid surface. The adsorption of a surfactant markedly changes the corrosion resisting property of a metal and for these reasons studies of the relation between adsorption and corrosion inhibition are considerable importance [81-84]. In the study of corrosion inhibition by surfactant, the critical micelle concentration (CMC) is the most important parameter. When the concentration of surfactant adsorbed on the solid surface is high enough, organized structures (hemi-micelles such as bi- or multilayer) are formed which decrease the corrosion reaction by blocking the metallic surface [85-90].

2.1. Synthesis of surfactants

2.1.1. Cationic quaternary ammonium fatty alkyl bromide surfactants

N,N-dimethylisopropyl amine (one mole) refluxed with alkyl halides (decyl-,dodecyl-and hexadecyl bromide)(one mole) in presence of acetone to give N,N,N,N-alkyldimethylisopropylammonium bromide.

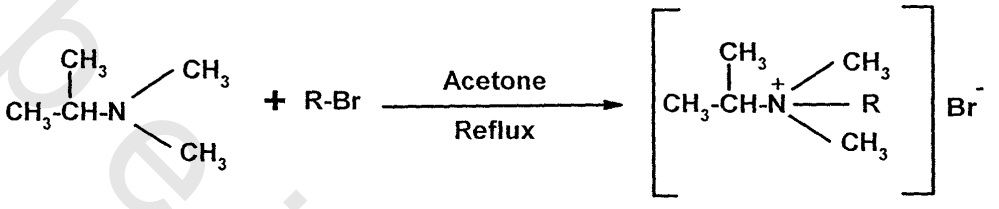

N,N-dimethylisopropyl amine

N,N,N,N-alkyldimethylisopropylammonium bromide

where, R= $CH_2(CH_2)_8CH_3$ (decane), $CH_2(CH_2)_{10}CH_3$ (dodecane), $CH_2(CH_2)_{14}CH_3$ (hexadecane).

2.1.2. Cationic quaternary ammonium fatty alkyl hydroxide surfactants

Potassium hydroxide pellets (one mole) refluxed with N,N,N,N-alkyl dimethylisopropylammonium bromide (one mole) in ethanol to give N,N,N,N-decyldimethylisopropylammonium hydroxide.

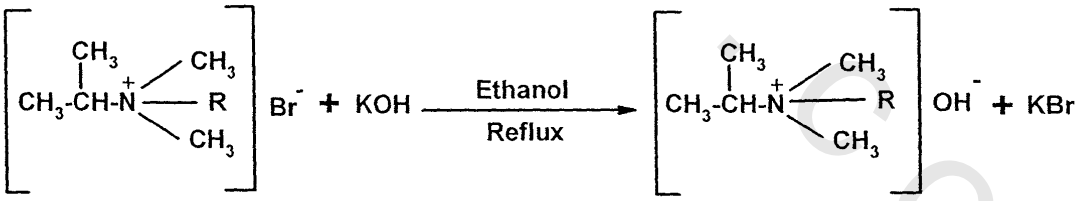

N,N,N,N-alkyldimethylisopropylammonium bromide

N,N,N,N-alkyldimethylisopropylammonium hydroxide

where, R= $CH_2(CH_2)_8CH_3$ (decane), $CH_2(CH_2)_{10}CH_3$ (dodecane), $CH_2(CH_2)_{14}CH_3$ (hexadecane).

2.1.3. Ethoxylation of cationic quaternary ammonium fatty alkyl bromide surfactants

P-N,N-dimethylaminobenzoic acid (one mole) was ethoxylated to give ethoxylated N,N-dimethylaminobenzoic acid then reacted with fatty alkyl bromide (dodecyl bromide)(one mole) in presence of acetone to give ethoxylated N,N,N,N-dodecyldimethylammonium bromide benzoic acid with 54, 64, 74 and 84 units.

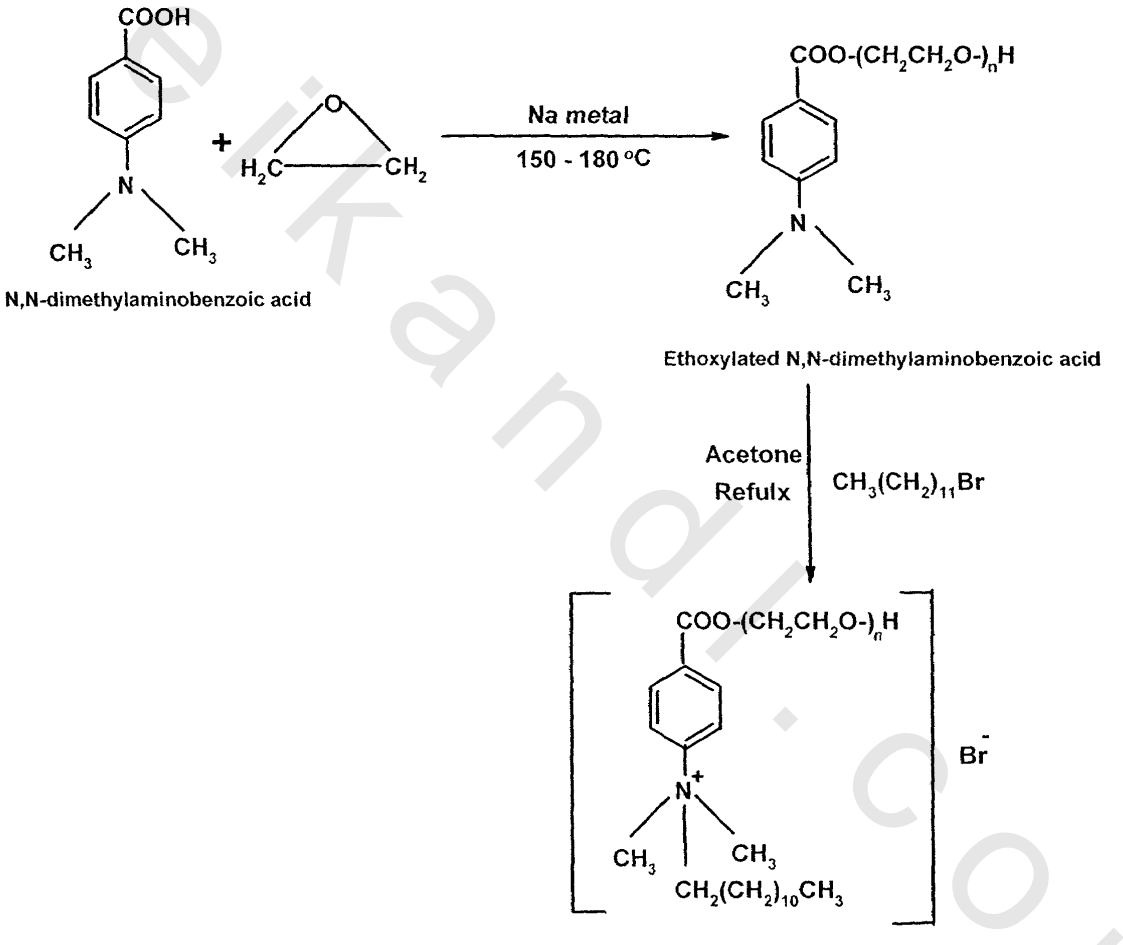

N,N-dimethylaminobenzoic acid

Ethoxylated N,N-dimethylaminobenzoic acid

Ethoxylated N,N,N,N-dodecyldimethylammonium bromide benzoic acid

where, n about 54, 64, 74, 84 units

2.2. Characterization of the synthesized surfactants

The chemical structures of the prepared surfactants were confirmed by the FT-IR and ^{1}HNMR spectra as shown in **Figs (17-22)**.

Table (2): FT-IR and ^{1}HMR spectral data for synthesized compounds

Compound Name	FT-IR (KBr) (cm^{-1})	^{1}HNMR (DMSO) (ppm)
DEDIABr	720.25 (CH_2 rocking bending), 1384.74 (CH_3 deformation bending), 1466.34 (CH_2 asym. bending), 2849.46 (CH_2 sym. stretch), 2918.55 (CH_2 asym. stretch), 2689.24 (N^+-C).	0.89 (t, 3H, $NCH_2CH_2(CH_2)_7C\underline{H}_3$), 1.27 (m, 5H, $NCH_2CH_2(C\underline{H}_2)_7CH_3$), 1.68 (m, 3H, $NCH_2C\underline{H}_2(CH_2)_7CH_3$), 3.23 (t, 3H, $NC\underline{H}_2CH_2(CH_2)_7CH_3$), 3.27 (s, 1H, $NC\underline{H}_3$), 3.69 (m, 7H, $NC\underline{H}(CH_3)_2$), 1.34 (d, 2H, $NCH(C\underline{H}_3)_2$), 2.94 (DMSO).
DODIABr	718.94 (CH_2 rocking bending), 1383.78 (CH_3 deformation bending), 1467.70 (CH_2 asym. bending), 2848.87 (CH_2 sym. stretch), 2916.95 (CH_2 asym. stretch), 2682.18 (N^+-C).	0.87 (t, 3H, $NCH_2CH_2(CH_2)_9C\underline{H}_3$), 1.25 (m, 5H, $NCH_2CH_2(C\underline{H}_2)_9CH_3$), 1.66 (m, 3H, $NCH_2C\underline{H}_2(CH_2)_9CH_3$), 3.24 (t, 3H, $NC\underline{H}_2CH_2(CH_2)_9CH_3$), 3.31 (s, 1H, $NC\underline{H}_3$), 3.68 (m, 7H, $NC\underline{H}(CH_3)_2$) , 1.29 (d, 2H, $NCH(C\underline{H}_3)_2$), 2.94 (DMSO).
HEDIABr	717.97 (CH_2 rocking bending), 1383.52 (CH_3 deformation bending), 1467.50 (CH_2 asym. bending), 2847.55 (CH_2 sym. stretch), 2916.86 (CH_2 asym. stretch), 2684.95 (N^+-C).	0.87 (t, 3H, $NCH_2CH_2(CH_2)_{13}C\underline{H}_3$), 1.24 (m, 5H, $NCH_2CH_2(C\underline{H}_2)_{13}CH_3$), 1.66 (m, 3H, $NCH_2C\underline{H}_2(CH_2)_{13}CH_3$), 3.21 (t, 3H, $NC\underline{H}_2CH_2(CH_2)_{13}CH_3$), 3.28 (s, 1H, $NC\underline{H}_3$), 3.67 (m, 7H, $NC\underline{H}(CH_3)_2$), 1.29 (d, 2H, $NCH(C\underline{H}_3)_2$), 2.93 (DMSO).
DEDIAOH	718.40 (CH_2 rocking bending), 1389.20 (CH_3 deformation bending), 1467.50 (CH_2 asym. bending), 2850.33 (CH_2 sym. stretch), 2921.26 (CH_2 asym. stretch), 2629.33 (N^+-C).	0.88 (t, 3H, $NCH_2CH_2(CH_2)_7C\underline{H}_3$), 1.25 (m, 5H, $NCH_2CH_2(C\underline{H}_2)_7CH_3$), 1.65 (m, 3H, $NCH_2C\underline{H}_2(CH_2)_7CH_3$), 3.25 (t, 3H, $NC\underline{H}_2CH_2(CH_2)_7CH_3$), 3.31 (s, 1H, $NC\underline{H}_3$), 3.68 (m, 7H, $NC\underline{H}(CH_3)_2$), 1.30 (d, 2H, $NCH(C\underline{H}_3)_2$), 2.93 (DMSO).

DODIAOH	708.40 (CH_2 rocking bending), 1405.04 (CH_3 deformation bending), 1465.48 (CH_2 asym. bending), 2848.68 (CH_2 sym. stretch), 2920.78 (CH_2 asym. stretch), 2629.33 (N^+-C).	0.87 (t, 3H, $NCH_2CH_2(CH_2)_9C\underline{H}_3$), 1.24 (m, 5H, $NCH_2CH_2(C\underline{H}_2)_9CH_3$), 1.66 (m, 3H, $NCH_2C\underline{H}_2(CH_2)_9CH_3$), 3.24 (t, 3H, $NC\underline{H}_2CH_2(CH_2)_9CH_3$), 3.28 (s, 1H, $NC\underline{H}_3$), 3.69 (m, 7H, $NC\underline{H}(CH_3)_2$), 1.31 (d, 2H, $NCH(C\underline{H}_3)_2$), 2.94 (DMSO).
HEDIAOH	712.54 (CH_2 rocking bending), 1393.75 (CH_3 deformation bending), 1462.84 (CH_2 asym. bending), 2849.33 (CH_2 sym. stretch), 2919.22 (CH_2 asym. stretch), 2643.63 (N^+-C).	0.88 (t, 3H, $NCH_2CH_2(CH_2)_{13}C\underline{H}_3$), 1.24 (m, 5H, $NCH_2CH_2(C\underline{H}_2)_{13}CH_3$), 1.66 (m, 3H, $NCH_2C\underline{H}_2(CH_2)_{13}CH_3$), 3.21 (t, 3H, $NC\underline{H}_2CH_2(CH_2)_{13}CH_3$), 3.25 (s, 1H, $NC\underline{H}_3$), 3.66 (m, 7H, $NC\underline{H}(CH_3)_2$), 1.29 (d, 2H, $NCH(C\underline{H}_3)_2$), 2.92 (DMSO).
E(54)	756.83 (CH_2 rocking bending), 1108.04 (C-O-C) ethereal band, 1246.28 (C-O stretch), 1349.30 (CH_3 deformation bending), 1459.87 (CH_2 asym. bending), 1541.54 (C=C stretch), 1732 (C=O stretch), 2624.12 (N^+-C), 2868.25 (CH_2 sym. stretch), 3380 (OH stretch).	0.85 (t, 3H, $NCH_2CH_2(CH_2)_8CH_2C\underline{H}_3$), 1.07 (m, 6H, $NCH_2CH_2(CH_2)_8C\underline{H}_2CH_3$), 1.17 (m, 5H, $NCH_2CH_2(C\underline{H}_2)_8CH_2CH_3$), 1.69 (m, 3H, $NCH_2C\underline{H}_2(CH_2)_8CH_2CH_3$), 3.25 (t, 3H, $NC\underline{H}_2CH_2(CH_2)_8CH_2CH_3$), 3.31 (s, 1H, $NC\underline{H}_3$), 7.30 (d, 2H, o-benzoic acid nucleus), 7.89 (d, 2H, m-benzoic acid nucleus), 3.75 (t, 3H, $COO(CH_2C\underline{H}_2O)(CH_2CH_2O\text{-})_nH$), 4.16 (t, 3H, $COO(C\underline{H}_2CH_2O)(CH_2CH_2O\text{-})_nH$), 3.39-3.49 (t, 3H, $COO(CH_2CH_2O)(C\underline{H}_2CH_2O\text{-})_nH$), 2.50 (s, 1H, $COO(CH_2CH_2O)(CH_2CH_2O\text{-})_n\underline{H}$), 2.98 (DMSO).
E(64)	750.36 (CH_2 rocking bending), 1111.55 (C-O-C) ethereal band, 1244.21 (C-O stretch), 1348.99 (CH_3 deformation bending), 1462.40 (CH_2 asym. bending), 1541.54 (C=C stretch), 1742.43 (C=O stretch), 2693.72 (N^+-C), 2880.17 (CH_2 sym. stretch), 3408.53 (OH stretch).	0.84 (t, 3H, $NCH_2CH_2(CH_2)_8CH_2C\underline{H}_3$), 1.03 (m, 6H, $NCH_2CH_2(CH_2)_8C\underline{H}_2CH_3$), 1.22 (m, 5H, $NCH_2CH_2(C\underline{H}_2)_8CH_2CH_3$), 1.66 (m, 3H, $NCH_2C\underline{H}_2(CH_2)_8CH_2CH_3$), 3.24 (t, 3H, $NC\underline{H}_2CH_2(CH_2)_8CH_2CH_3$), 3.29 (s, 1H, $NC\underline{H}_3$), 3.57 (t, 3H, $COO(CH_2C\underline{H}_2O)(CH_2CH_2O\text{-})_nH$), 4.25 (t, 3H, $COO(C\underline{H}_2CH_2O)(CH_2CH_2O\text{-})_nH$), 3.39-3.49 (t, 3H, $COO(CH_2CH_2O)(C\underline{H}_2CH_2O\text{-})_nH$), 2.50 (s, 1H , $COO(CH_2CH_2O)(CH_2CH_2O\text{-})_n\underline{H}$), 2.98 (DMSO).

E(74)	748.46 (CH_2 rocking bending), 1111.66 (C-O-C) ethereal band, 1241.12 (C-O stretch), 1348.09 (CH_3 deformation bending), 1463.42 (CH_2 asym. bending), 1625.10 (C=C stretch), 1739.11 (C=O stretch), 2692.58 (N^+-C), 2882.13 (CH_2 sym. stretch), 3379.99 (OH stretch).	0.87 (t, 3H, $NCH_2CH_2(CH_2)_8CH_2C\underline{H}_3$), 1.05 (m, 6H, $NCH_2CH_2(CH_2)_8C\underline{H}_2CH_3$), 1.24 (m, 5H, $NCH_2CH_2(C\underline{H}_2)_8CH_2CH_3$), 1.67 (m, 3H, $NCH_2C\underline{H}_2(CH_2)_8CH_2CH_3$), 3.23 (t, 3H, $NC\underline{H}_2CH_2(CH_2)_8CH_2CH_3$), 3.27 (s, 1H, $NC\underline{H}_3$), 3.58 (t, 3H, $COO(CH_2C\underline{H}_2O)(CH_2CH_2O\text{-})_nH$), 4.32 (t, 3H, $COO(C\underline{H}_2CH_2O)(CH_2CH_2O\text{-})_nH$), 3.39-3.47 (t, 3H, $COO(CH_2CH_2O)(C\underline{H}_2CH_2O\text{-})_nH$), 2.49 (s, 1H, $COO(CH_2CH_2O)(CH_2CH_2O\text{-})_n\underline{H}$), 2.97 (DMSO).
E(84)	745.85 (CH_2 rocking bending), 1109.31 (C-O-C) ethereal band, 1239.98 (C-O stretch), 1349.10 (CH_3 deformation bending), 1465.95 (CH_2 asym. bending), 1565.84 (C=C stretch), 1734.27 (C=O stretch), 2693.80 (N^+-C), 2883.65 (CH_2 sym. stretch), 3398.98 (OH stretch).	0.86 (t, 3H, $NCH_2CH_2(CH_2)_8CH_2C\underline{H}_3$), 1.04 (m, 6H, $NCH_2CH_2(CH_2)_8C\underline{H}_2CH_3$), 1.25 (m, 5H, $NCH_2CH_2(C\underline{H}_2)_8CH_2CH_3$), 1.69 (m, 3H, $NCH_2C\underline{H}_2(CH_2)_8CH_2CH_3$), 3.26 (t, 3H, $NC\underline{H}_2CH_2(CH_2)_8CH_2CH_3$), 3.31 (s, 1H, $NC\underline{H}_3$), 3.55 (t, 3H, $COO(CH_2C\underline{H}_2O)(CH_2CH_2O\text{-})_nH$), 4.28 (t, 3H, $COO(C\underline{H}_2CH_2O)(CH_2CH_2O\text{-})_nH$), 3.38-3.49 (t, 3H, $COO(CH_2CH_2O)(C\underline{H}_2CH_2O\text{-})_nH$), 2.51 (s, 1H, $COO(CH_2CH_2O)(CH_2CH_2O\text{-})_n\underline{H}$), 2.99 (DMSO).

For cationic surfactants, the data of ^{1}HNMR spectra confirmed the expected hydrogen proton distribution in the synthesized cationic surfactants. All prepared compounds have the same signals. The only difference between the signals of these compounds is the signal intensity of methylene proton (t, 6H, $NCH_2CH_2(C\underline{H}_2)_nCH_3$), where the intensity of this signal increases by increasing the methylene groups (chain length) of the prepared compounds.

For ethoxylated-cationic surfactant, all compounds have the same signals and the only difference between the signals of these compounds is the signals intensity of ethereal proton (t, 3H, $COO(CH_2CH_2O)(C\underline{H}_2CH_2O)_n$), where the intensity of this signal increases by increasing ethylene oxide units. Also by increasing of ethylene oxide units, signals (d, 2H, o-benzoic acid nucleus), (d, 2H, m-benzoic acid nucleus) are decrease until disappeared from 64 to 84 units.

2.3. Surface properties of the prepared surfactants

2.3.1. The surface tension (γ) and critical micelle concentration (CMC).

Most organic corrosion inhibitors are adsorbed on the metal/solution interface by displacing water molecules from the surface and forming a compact barrier film. The ability of a surfactant molecule to adsorb is generally directly related to its ability to aggregate and form micelles. There is equilibrium between the singly adsorbed surfactant molecules. The equilibrium occurred at the concentration of complete surface saturation. The micelle formation is the most vital point of view in the surfactant fundamental because it is the most effective geometrical arrangement of the molecules at the desired concentration [91, 92]. Below CMC, individual surfactant molecules or monomers tend to adsorb on exposed interfaces, so interfacial aggregation reduces surface tension and is related to corrosion inhibition. The surface tension (γ) of surfactants was measured for a range of concentrations above and below the critical micelle concentration (CMC). A representative plot of γ versus concentration for N,N,N,N-alkyldimethylisopropylammonium bromide is shown in **Fig. (23)** and for N,N,N,N-alkyldimethylisopropylammonium hydroxid is shown in **Fig. (24),** while ethoxylated N,N,N,N-dodecyldimethylammonium bromide benzoic acid with 54, 64, 74 and 84 units are shown in **Fig. (25)**. Linear decrease in surface tension was observed with the increase of surfactant concentrations [93]. This is a common behavior shown by surfactants in solution and is used to determine their purity and CMC's. The CMC values were obtained from the break point in γ–log C plots are shown in **Figs. (23-25)** and listed in **Table (3)**. The γ–log C plots also provide information about minimum area

per molecule at air/water interface, effectiveness and maximum surface excess concentration of surfactant ions of the synthesized surfactants.

For cationic surfactants, a comparison of CMC for homologous series of surfactant demonstrates that, increasing the length of the hydrocarbon chain has the tendency of lowering the concentration at which aggregation is initiated, owing to enhanced hydrophobic interaction between the counter ion and micellar core. Increasing the length of the hydrocarbon chain increases the average micellar aggregation number [94, 95] as shown in **Figs. (23, 24)**.

For ethoxylated-cationic surfactants, it can be observed that an increase in the ethoxylation degree from 54 to 84 EO reduces the CMC value. This occurs due to the increase in the hydrophilic portion of the surfactant molecule, making the radius and surface area of micelle larger, a condition that favors micellization at relatively lower concentrations [96] as shown in **Fig. (25)**.

2.3.2. Effectiveness (Π_{CMC})

The effectiveness of the surfactant solution **(Π_{CMC})** is defined as the difference between the surface tension at the critical micelle concentration (γ_{CMC}) and that for the bi-distilled water (γ_o) at constant temperature [97].

$$\Pi_{CMC} = \gamma_o - \gamma_{CMC} \qquad (7)$$

where γ_o and γ_{CMC} are the surface tensions of pure water and surface tension at CMC, respectively.

Π_{CMC} values were listed in **Table (3)**. It was found that, effectiveness increases with the increase of alkyl chain length and the weak binding ability of the counter ion.

2.3.3. Maximum surface excess (Γ_{max})

Maximum surface excess (Γ_{max}) is defined as the effectiveness of adsorption at an interface. The maximum surface excess concentration of surfactant ions, Γ_{max}, was calculated from the slope of the straight line in the surface tension plot (dγ/d lnC) below CMC, using appropriate form of Gibbs adsorption equation [98, 99]:

$$\Gamma_{max} = -(1/nRT)(d\gamma/d\ lnC) \qquad (8)$$

where Γ_{max} is the maximum surface excess concentration of surfactant ions, R is the gas constant, T is the absolute temperature, C is the concentration of surfactant, γ is the surface tension at given concentration and n is the number of species ions in solution.

Pumping of surfactant molecules to the boundary surfaces between phases to form adsorbed layer is one of the most objective application of surfactants as a vital branch of chemistry in several application [100, 101].

The values of maximum surface excess concentration were calculated and listed in **Table (3)**.

For cationic surfactants, it was found that maximum surface excess concentration decrease by increasing carbon chain length due to hydrophobic effect of carbon chain.

For ethoxylated-cationic surfactants, it was found that maximum surface excess concentration decrease by increasing carbon chain length due to hydrophilic effect of poly ethylene oxide units, the maximum value of the maximum surface excess concentration corresponds to the maximum concentration that a surfactant can attain at the interface.

2.3.4. Minimum area per molecule (A_{min})

The minimum surface area per adsorbed molecule, A_{min}, can be obtained as follows [102]:

$$A_{min} = 10^{16} / \Gamma_{max} N_A \qquad (9)$$

where N_A is the Avogadro's number and Γ_{max} (mol m^{-2}) is the maximum surface excess of adsorbed surfactant molecules at the interface.

The values of area per molecule for the prepared surfactants were calculated and listed in **Table (3)**.

For cationic surfactants, it was found that the same head group area but with different carbon chain length, the area values increased by increase the carbon chain length [103].

For ethoxylated-cationic surfactants, the EO group constitutes the polar head of these surfactants and its increase means increasing surface area occupied by each surfactant molecule, being necessary less surfactant molecules to saturate the interface, as can be observed in **Table (3)**.

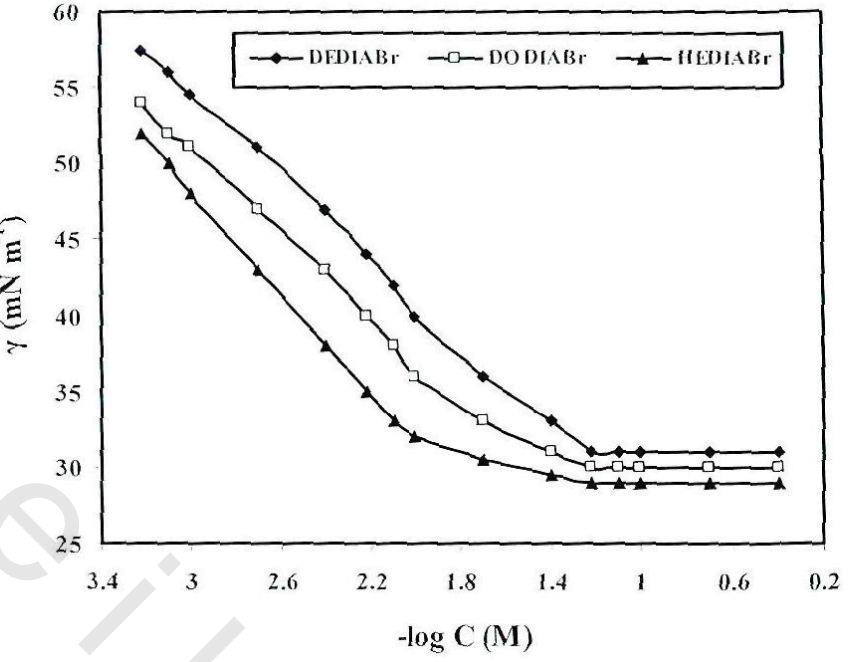

Fig. (23): Variation of the surface tension with logarithm of concentrations for synthesized N,N,N,N-alkyldimethylisopropylammonium bromide in water at 30 °C.

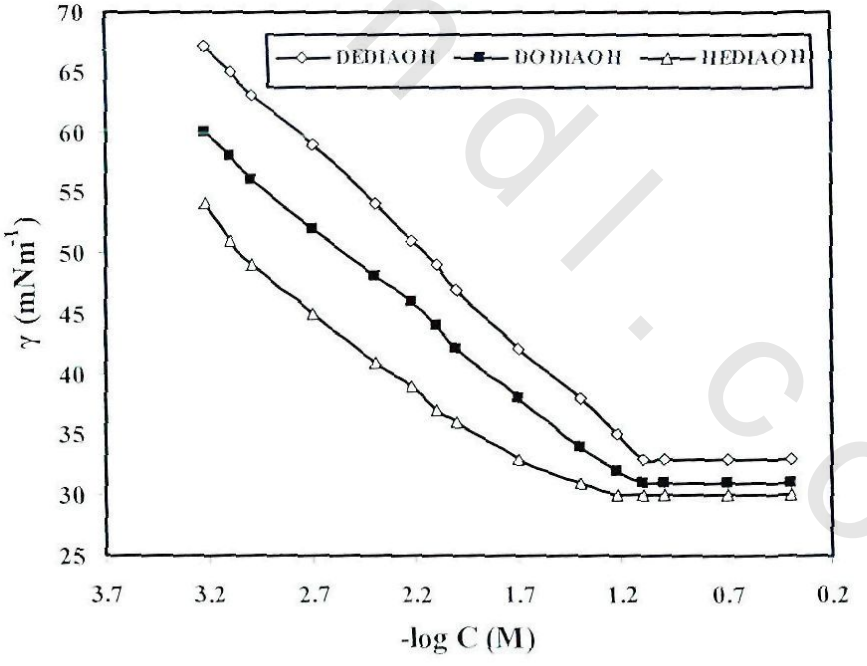

Fig. (24): Variation of the surface tension with logarithm of concentrations for synthesized N,N,N,N-alkyldimethylisopropylammonium hydroxide in water at 30 °C.

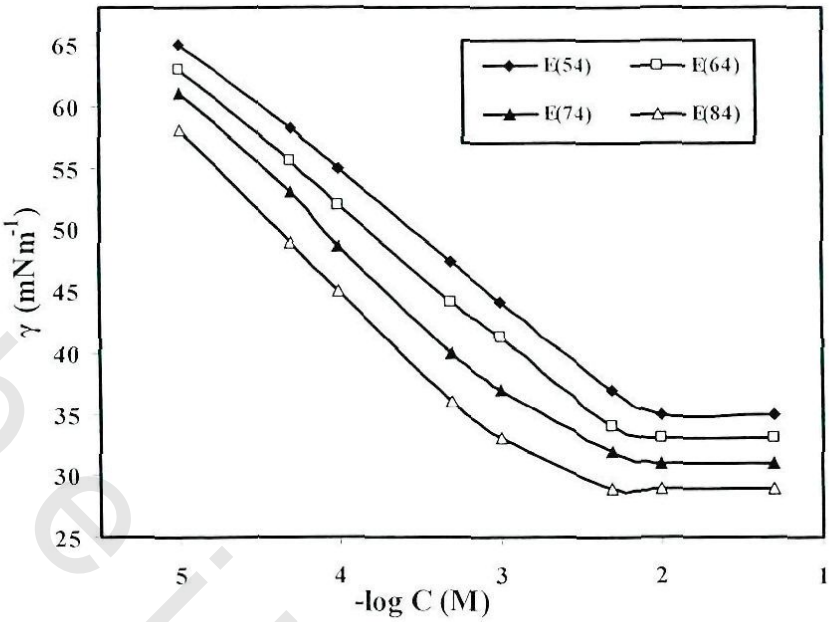

Fig. (25): Variation of the surface tension with logarithm of concentrations for synthesized ethoxylated N,N,N,N-dodecyldimethylammonium bromide benzoic acid with 54, 64, 74, 84 units in water at 30 °C.

Table (3): The critical micelle concentration (CMC) and surface parameters of the prepared surfactants from surface tension measurements at 30 °C

Sample	CMC x 10^2 M	γ_{CMC} mNm^{-1}	Π_{CMC} $mol\ dm^{-3}$	Γ_{max} x 10^{10} $mol\ cm^{-2}$	A_{min} nm^2
DEDIABr	2.300	33.1	38.9	1.11	1.50
DODIABr	1.500	30.0	42.0	1.02	1.63
HEDIABr	0.900	28.6	43.4	0.95	1.74
DEDIAOH	2.500	31.5	40.5	1.50	1.11
DODIAOH	1.870	30.9	41.1	1.32	1.26
HEDIAOH	0.900	29.7	42.3	1.19	1.39
E(54)	0.164	34.8	37.2	1.13	1.48
E(64)	0.135	32.4	39.6	1.01	1.64
E(74)	0.102	29.6	42.4	0.94	1.77
E(84)	0.073	25.9	46.1	0.85	1.95

2.4. Conductivity measurements

Specific conductivity (K) measurements were performed for the prepared surfactants at 30 °C in order to evaluate the CMC and the degree of counter ion dissociation, β. It is well known that the specific conductivity is linearly correlated to the surfactant concentration in both the premicellar and in the postmicellar regions and the slope in the premicellar region greater than that in the postmicellar region [104]. The intersection point between the two straight lines gives the CMC while the ratio between the slopes of the postmicellar region to that in the premicellar region gives counter ion dissociation.

The relation between specific conductivity and concentration of the synthesized N,N,N,N-alkyldimethylisopropylammonium bromide, N,N,N, N-alkyldimethylisopropylammonium hydroxide and the ethoxylated N,N,N,N-dodecyldimethylammonium bromide benzoic acid with 54, 64, 74 and 84 units were shown in **Figs. (26-28)**. Values of degree of counter ion dissociation were calculated and listed in **Table (4)**.

Results were showed that, for cationic surfactants, the degree of dissociation of surfactants increase by increasing carbon chain length due to the variation in the electronic charge density on the central nitrogen atom, which depends on the positive inductive effect of the alkyl group and bulkiness of cation.

For ethoxylated-cationic surfactants, it can be observed that the dissociation degree of surfactants increase by increasing ethoxylation degree from 54 to 84 EO unit due to hydrophilic part increase.

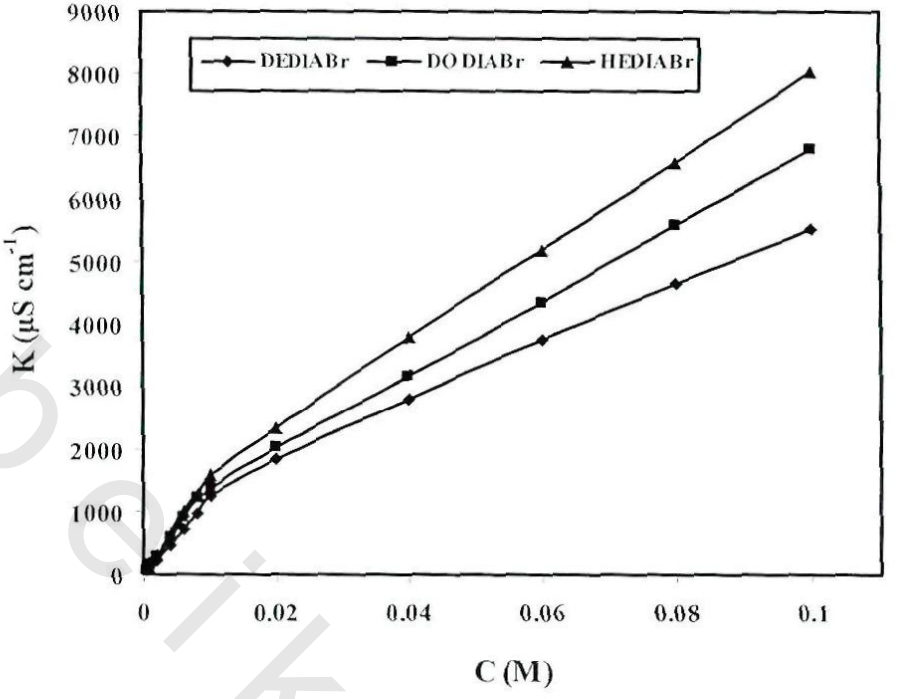

Fig. (26): The plots of specific conductivity, K, against concentration for synthesized N,N,N,N-alkyldimethylisopropylammonium bromide in water at 30 °C.

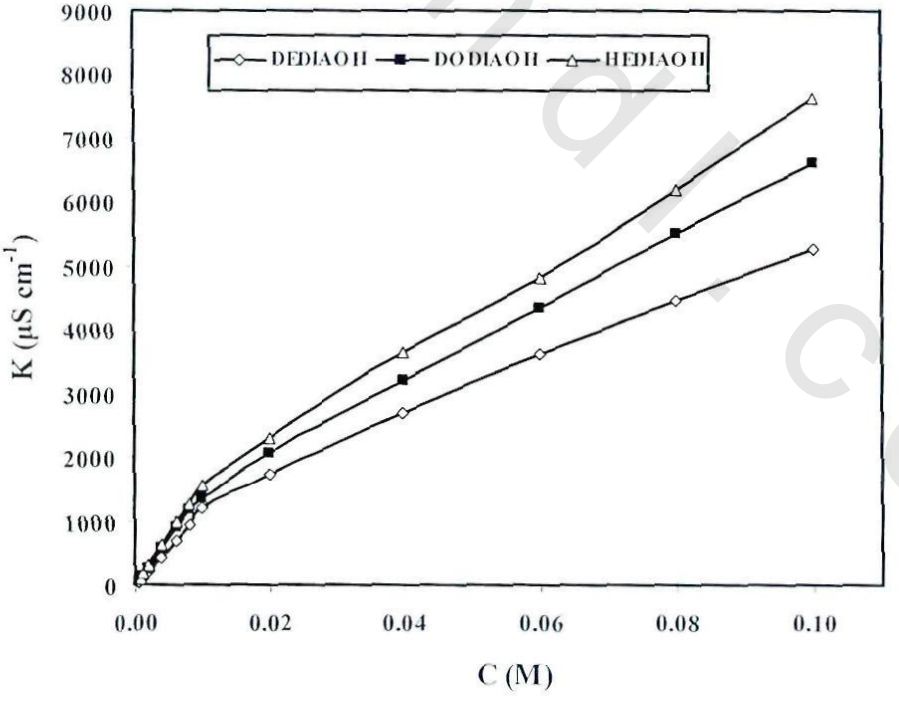

Fig. (27): The plots of specific conductivity, K, against concentration for synthesized N,N,N,N-alkyldimethylisopropylammonium hydroxide in water at 30 °C.

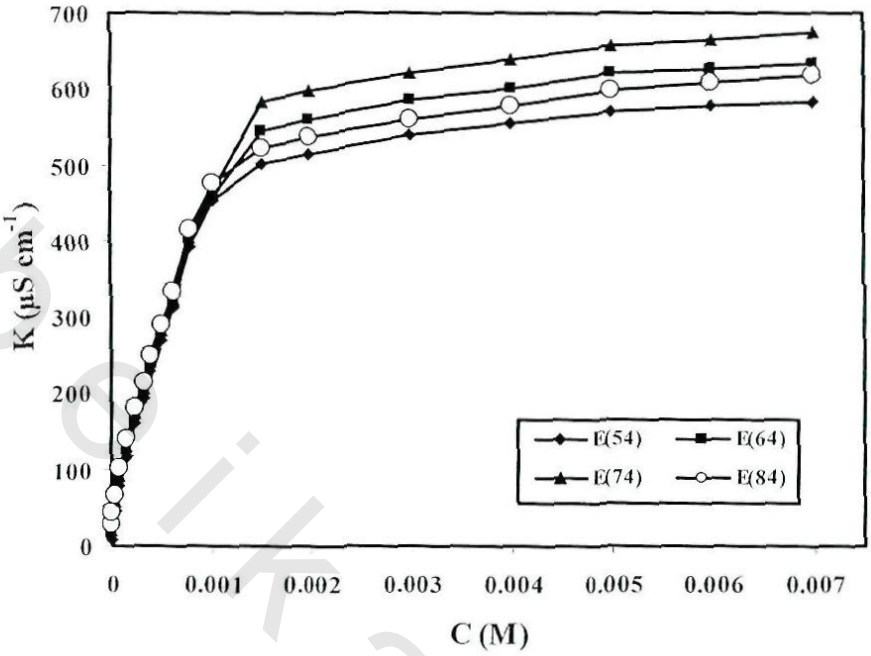

Fig. (28): The plots of specific conductivity, K, against concentration for synthesized ethoxylated N,N,N,N-dodecyldimethylammonium bromide benzoic acid with 54, 64, 74, 84 units in water at 30 °C.

Table (4): The critical micelle concentration (CMC), degree of dissociation and free energy of micellization of the prepared surfactants from specific conductivity measurements at 30 °C

Compound	CMC x 10^2 M	β	ΔG_{mic} kJ mol^{-1}
DEDIABr	2.320	0.376	-15.40
DODIABr	1.520	0.414	-16.74
HEDIABr	0.860	0.447	-18.61
DEDIAOH	2.500	0.358	-15.26
DODIAOH	1.840	0.393	-16.17
HEDIAOH	0.900	0.414	-18.82
E(54)	0.162	0.150	-29.88
E(64)	0.138	0.180	-30.27
E(74)	0.103	0.210	-31.07
E(84)	0.079	0.250	-31.86

2.5. The standard free energy of micelle formation ΔG^{o}_{m}

The CMC of a surfactant is regarded as a measure of the stability of its micellar form relative to its monomeric form. In the charged pseudophase model of micelle formation, the standard free energy of micelle formation per mole of surfactant is given by equation:

$$\Delta G^{o}_{m} = (2 - \beta)\, RT \ln (CMC) \qquad (10)$$

where R is the gas constant, T is the absolute temperature and CMC is expressed in the molarity of the surfactant.

For cationic surfactants, it is clear that the ΔG^{o}_{m} values increase in the negative value as the carbon chain length of the prepared surfactants increase; this means that the micelle formation is thermodynamically favored for surfactant which has longer carbon chain and micellization process proceeds spontaneously.

For ethoxylated-cationic surfactants, the low values of the Gibbs free energy with increasing head group chain length indicate the influence of this parameter in the micellization process.

2.6. Gravimetric measurements

The corrosion rate (k) was calculated from the following equation [105]:

$$k = (W/St) \qquad (11)$$

where W is the average weight loss of three parallel carbon steel sheets, S is the total area of the specimen, and t is the immersion time.

Inhibition efficiency (η_w%) and surface coverage (θ) for synthesized surfactants were calculated according to the following equations [106] :

$$\eta_w\ \% = [\{W_{corr} - W_{corr}(inh)\}/\ W_{corr}] \times 100 \qquad (12)$$

$$\theta = \{W_{corr} - W_{corr}(inh)\}/\ W_{corr} \qquad (13)$$

where W_{corr} and $W_{corr}(inh)$ are the weight loss of carbon steel in absence and presence of the inhibitors, respectively.

Corrosion rate values of carbon steel in 1M HCl in absence and presence of various concentrations of N,N,N,N-alkyldimethylisopropylammonium bromide inhibitors, N,N,N,N-alkyldimethylisopropylammonium hydroxide inhibitors and ethoxylated N,N,N,N-dodecyldimethylammonium bromide benzoic acid corrosion inhibitors with 54, 64, 74, 84 units were calculated and recorded in **Tables (5-14).**

For all cationic surfactants, results show that the corrosion inhibition efficiencies increase with increasing inhibitor concentrations [107,108], as shown in **Figs. (29, 30)**. This due to the surface converge of the carbon steel was increasing by increase of inhibitor concentration. The obtained results indicate that, inhibition efficiency increased by increasing of alkyl chain length because of hydrophobicity and surface coverage of the prepared surfactants increased.

Results show that, the corrosion inhibition efficiency of N,N,N,N-alkyldimethylisopropylammonium bromide is more than N,N,N,N-alkyldimethylisopropylammonium hydroxide at the same alkyl chain length due to the electronegativity and the bulkness of bromide ion are more than in hydroxide ion.

For ethoxylated-cationic surfactants, the results show that the corrosion inhibition efficiency increases with increasing inhibitor concentrations as shown in **Fig. (31)**. This due to the surface converge of the carbon steel was increasing by inhibitor concentration increase. Also, the inhibition efficiencies increase with increasing the ethoxylation degree from 54 to 84 EO units. The increase in length of the hydrocarbon chain in the inhibitor molecule means more bulky molecule, which protects the surface from attack and hence reduces the rate of corrosion [109].

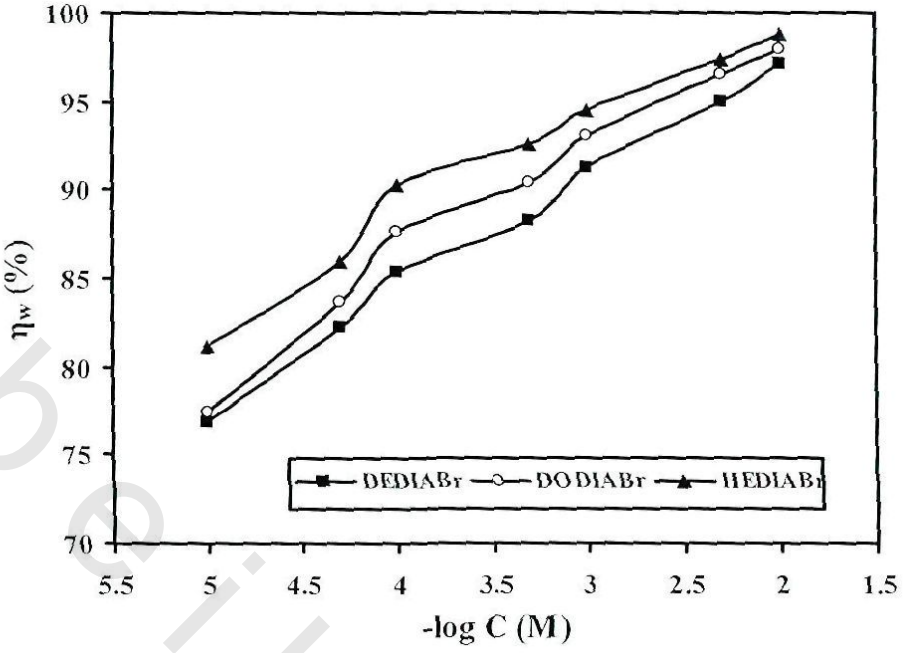

Fig. (29): Variation of the corrosion inhibition efficiency with logarithmic concentrations of the synthesized N,N,N,N-alkyldimethyl-isopropylammonium bromide in 1M HCl at 30 °C.

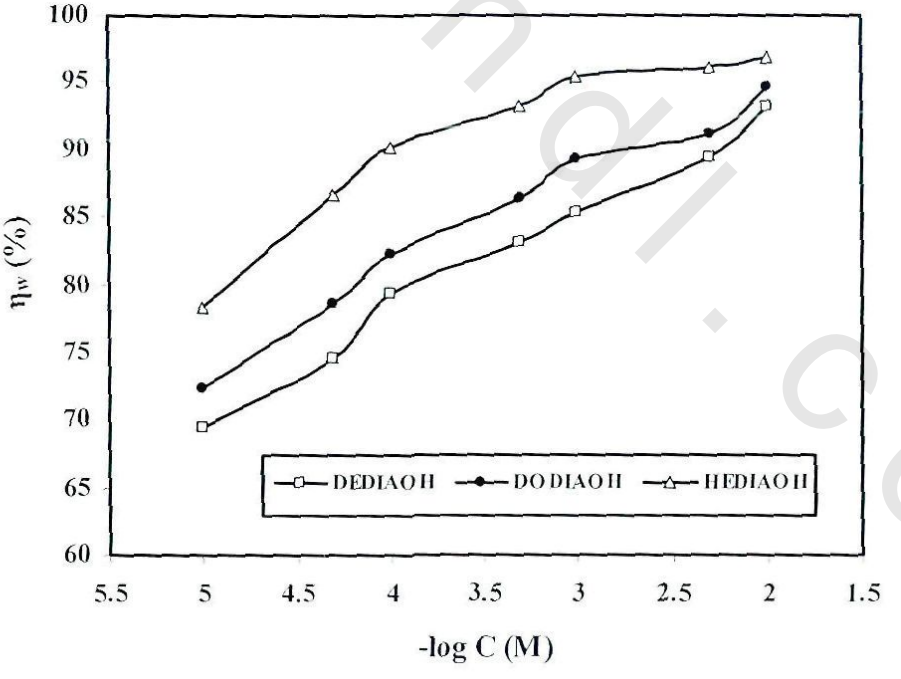

Fig. (30): Variation of the corrosion inhibition efficiency with logarithmic concentrations of the synthesized N,N,N,N-alkyldimethylisopropyl-ammonium hydroxide in 1M HCl at 30 °C.

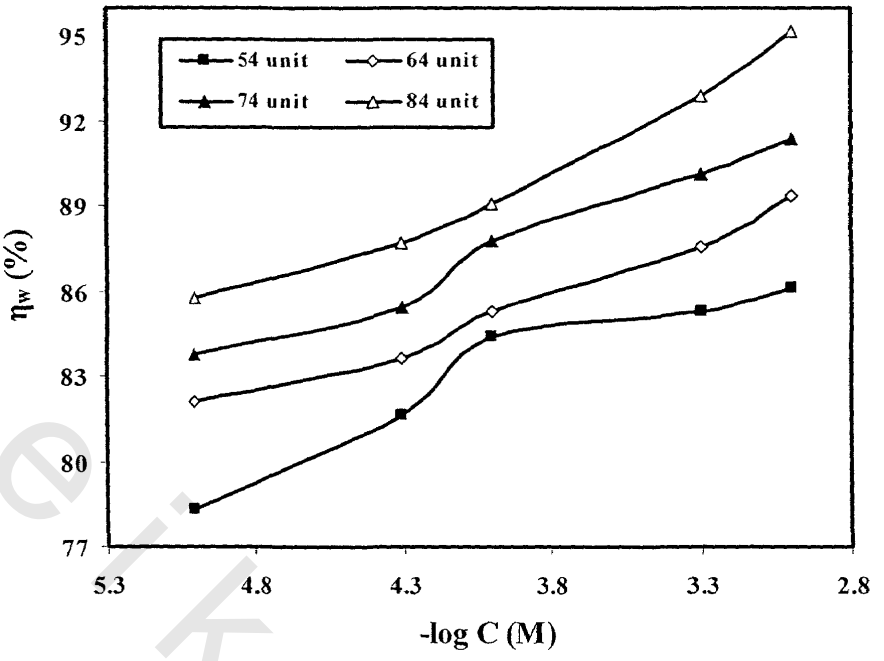

Fig. (31): Variation of the corrosion inhibition efficiency with logarithmic concentrations of the synthesized ethoxylated N,N,N,N-dodecyl-dimethylammonium bromide benzoic acid with 54, 64, 74, 84 units in 1M HCl at 30 °C.

Table (5): Corrosion rate of carbon steel, surface coverage and corrosion inhibition efficiency in absence and presence of different concentrations of DEDIABr in 1M HCl from gravimetric measurements at various temperatures

Temperature °C	Conc. of inhibitor M	Corrosion Rate mg cm^{-2} h^{-1}	θ	η_w %
30	0.00	0.196	-	-
	$1x10^{-5}$	0.045	0.77	76.8
	$5x10^{-5}$	0.035	0.82	82.2
	$1x10^{-4}$	0.029	0.85	85.4
	$5x10^{-4}$	0.023	0.88	88.2
	$1x10^{-3}$	0.017	0.91	91.3
	$5x10^{-3}$	0.010	0.95	94.9
	$1x10^{-2}$	0.006	0.97	97.1
40	0.00	0.402	-	-
	$1x10^{-5}$	0.143	0.64	64.3
	$5x10^{-5}$	0.114	0.72	71.7
	$1x10^{-4}$	0.103	0.74	74.3
	$5x10^{-4}$	0.087	0.78	78.3
	$1x10^{-3}$	0.063	0.84	84.4
	$5x10^{-3}$	0.043	0.89	89.4
	$1x10^{-2}$	0.031	0.92	92.4
50	0.00	0.829	-	-
	$1x10^{-5}$	0.386	0.53	53.4
	$5x10^{-5}$	0.329	0.60	60.3
	$1x10^{-4}$	0.289	0.65	65.1
	$5x10^{-4}$	0.248	0.70	70.1
	$1x10^{-3}$	0.190	0.77	77.1
	$5x10^{-3}$	0.140	0.83	83.1
	$1x10^{-2}$	0.113	0.86	86.4

Table (6): Corrosion rate of carbon steel, surface coverage and corrosion inhibition efficiency in absence and presence of different concentrations of DODIABr in 1M HCl from gravimetric measurements at various temperatures

Temperature °C	Conc. of inhibitor M	Corrosion Rate mg cm^{-2} h^{-1}	θ	η_w %
30	0.00	0.196	-	-
	$1x10^{-5}$	0.044	0.77	77.4
	$5x10^{-5}$	0.032	0.84	83.7
	$1x10^{-4}$	0.024	0.88	87.6
	$5x10^{-4}$	0.019	0.90	90.4
	$1x10^{-3}$	0.014	0.93	93.1
	$5x10^{-3}$	0.007	0.97	96.5
	$1x10^{-2}$	0.004	0.98	97.9
40	0.00	0.402	-	-
	$1x10^{-5}$	0.155	0.61	61.4
	$5x10^{-5}$	0.127	0.68	68.3
	$1x10^{-4}$	0.089	0.78	77.9
	$5x10^{-4}$	0.077	0.81	80.9
	$1x10^{-3}$	0.047	0.88	88.4
	$5x10^{-3}$	0.034	0.92	91.6
	$1x10^{-2}$	0.028	0.93	93.1
50	0.00	0.829	-	-
	$1x10^{-5}$	0.379	0.54	54.3
	$5x10^{-5}$	0.303	0.63	63.4
	$1x10^{-4}$	0.246	0.7	70.3
	$5x10^{-4}$	0.208	0.75	74.9
	$1x10^{-3}$	0.197	0.76	76.2
	$5x10^{-3}$	0.115	0.86	86.1
	$1x10^{-2}$	0.104	0.88	87.5

Table (7): Corrosion rate of carbon steel, surface coverage and corrosion inhibition efficiency in absence and presence of different concentrations of HEDIABr in 1M HCl from gravimetric measurements at various temperatures

Temperature °C	Conc. of inhibitor M	Corrosion Rate mg cm^{-2} h^{-1}	θ	η_w %
30	0.00	0.196	-	-
	$1x10^{-5}$	0.037	0.81	81.2
	$5x10^{-5}$	0.027	0.86	86.0
	$1x10^{-4}$	0.019	0.90	90.3
	$5x10^{-4}$	0.015	0.93	92.6
	$1x10^{-3}$	0.011	0.95	94.5
	$5x10^{-3}$	0.005	0.97	97.4
	$1x10^{-2}$	0.002	0.99	98.8
40	0.00	0.402	-	-
	$1x10^{-5}$	0.119	0.71	70.5
	$5x10^{-5}$	0.099	0.75	75.3
	$1x10^{-4}$	0.090	0.78	77.5
	$5x10^{-4}$	0.072	0.82	82.2
	$1x10^{-3}$	0.038	0.91	90.5
	$5x10^{-3}$	0.029	0.93	92.9
	$1x10^{-2}$	0.024	0.94	94.1
50	0.00	0.829	-	-
	$1x10^{-5}$	0.336	0.59	59.4
	$5x10^{-5}$	0.278	0.66	66.4
	$1x10^{-4}$	0.196	0.76	76.3
	$5x10^{-4}$	0.175	0.79	78.9
	$1x10^{-3}$	0.146	0.82	82.4
	$5x10^{-3}$	0.115	0.86	86.1
	$1x10^{-2}$	0.096	0.88	88.4

Table (8): Corrosion rate of carbon steel, surface coverage and corrosion inhibition efficiency in absence and presence of different concentrations of DEDIAOH in 1M HCl from gravimetric measurements at various temperatures

Temperature °C	Conc. of inhibitor M	Corrosion Rate mg cm^{-2} h^{-1}	θ	η_w %
30	0.00	0.196	-	-
	$1x10^{-5}$	0.060	0.69	69.4
	$5x10^{-5}$	0.050	0.75	74.5
	$1x10^{-4}$	0.040	0.79	79.4
	$5x10^{-4}$	0.033	0.83	83.1
	$1x10^{-3}$	0.029	0.85	85.3
	$5x10^{-3}$	0.021	0.89	89.4
	$1x10^{-2}$	0.013	0.93	93.2
40	0.00	0.402	-	-
	$1x10^{-5}$	0.167	0.58	58.4
	$5x10^{-5}$	0.149	0.63	62.8
	$1x10^{-4}$	0.136	0.66	66.2
	$5x10^{-4}$	0.106	0.74	73.6
	$1x10^{-3}$	0.089	0.78	77.8
	$5x10^{-3}$	0.062	0.85	84.6
	$1x10^{-2}$	0.051	0.87	87.4
50	0.00	0.829	-	-
	$1x10^{-5}$	0.414	0.50	50.1
	$5x10^{-5}$	0.370	0.55	55.4
	$1x10^{-4}$	0.337	0.59	59.3
	$5x10^{-4}$	0.295	0.64	64.4
	$1x10^{-3}$	0.270	0.67	67.4
	$5x10^{-3}$	0.206	0.75	75.1
	$1x10^{-2}$	0.163	0.80	80.3

Table (9): Corrosion rate of carbon steel, surface coverage and corrosion inhibition efficiency in absence and presence of different concentrations of DODIAOH in 1M HCl from gravimetric measurements at various temperatures

Temperature °C	Conc. of inhibitor M	Corrosion Rate mg cm^{-2} h^{-1}	θ	η_w %
30	0.00	0.196	-	-
	$1x10^{-5}$	0.054	0.72	72.4
	$5x10^{-5}$	0.042	0.79	78.7
	$1x10^{-4}$	0.035	0.82	82.2
	$5x10^{-4}$	0.027	0.86	86.4
	$1x10^{-3}$	0.021	0.89	89.2
	$5x10^{-3}$	0.017	0.91	91.1
	$1x10^{-2}$	0.010	0.95	94.7
40	0.00	0.402	-	-
	$1x10^{-5}$	0.162	0.60	59.6
	$5x10^{-5}$	0.139	0.65	65.4
	$1x10^{-4}$	0.121	0.70	69.9
	$5x10^{-4}$	0.103	0.74	74.3
	$1x10^{-3}$	0.077	0.81	81.0
	$5x10^{-3}$	0.047	0.88	88.4
	$1x10^{-2}$	0.041	0.90	89.9
50	0.00	0.829	-	-
	$1x10^{-5}$	0.388	0.53	53.2
	$5x10^{-5}$	0.345	0.58	58.4
	$1x10^{-4}$	0.296	0.64	64.3
	$5x10^{-4}$	0.244	0.71	70.5
	$1x10^{-3}$	0.211	0.75	74.5
	$5x10^{-3}$	0.179	0.78	78.4
	$1x10^{-2}$	0.140	0.83	83.1

Table (10): Corrosion rate of carbon steel, surface coverage and corrosion inhibition efficiency in absence and presence of different concentrations of HEDIAOH in 1M HCl from gravimetric measurements at various temperatures

Temperature °C	Conc. of inhibitor M	Corrosion Rate mg cm^{-2} h^{-1}	θ	η_w %
30	0.00	0.196	-	-
	$1x10^{-5}$	0.042	0.78	78.4
	$5x10^{-5}$	0.030	0.85	86.6
	$1x10^{-4}$	0.025	0.87	90.1
	$5x10^{-4}$	0.019	0.90	93.2
	$1x10^{-3}$	0.017	0.91	95.4
	$5x10^{-3}$	0.012	0.94	96.1
	$1x10^{-2}$	0.008	0.96	96.8
40	0.00	0.402	-	-
	$1x10^{-5}$	0.142	0.65	64.6
	$5x10^{-5}$	0.118	0.71	70.6
	$1x10^{-4}$	0.103	0.74	74.3
	$5x10^{-4}$	0.079	0.80	80.2
	$1x10^{-3}$	0.052	0.87	87.1
	$5x10^{-3}$	0.042	0.89	89.5
	$1x10^{-2}$	0.035	0.91	91.2
50	0.00	0.829	-	-
	$1x10^{-5}$	0.368	0.56	55.6
	$5x10^{-5}$	0.331	0.60	60.1
	$1x10^{-4}$	0.281	0.66	66.1
	$5x10^{-4}$	0.219	0.74	73.6
	$1x10^{-3}$	0.202	0.76	75.7
	$5x10^{-3}$	0.148	0.82	82.1
	$1x10^{-2}$	0.138	0.83	83.4

Table (11): Corrosion rate of carbon steel, surface coverage and corrosion inhibition efficiency in absence and presence of different concentrations of E(54) in 1M HCl from gravimetric measurements at various temperatures

Temperature °C	Conc. of inhibitor M	Corrosion Rate mg cm^{-2} h^{-1}	θ	η_w %
30	0.00	0.196	-	-
	$1x10^{-5}$	0.043	0.78	78.3
	$5x10^{-5}$	0.034	0.83	82.6
	$1x10^{-4}$	0.030	0.84	84.5
	$5x10^{-4}$	0.028	0.86	85.9
	$1x10^{-3}$	0.023	0.88	88.4
40	0.00	0.402	-	-
	$1x10^{-5}$	0.132	0.67	67.2
	$5x10^{-5}$	0.106	0.74	74.6
	$1x10^{-4}$	0.094	0.77	77.7
	$5x10^{-4}$	0.074	0.82	81.5
	$1x10^{-3}$	0.067	0.83	83.3
50	0.00	0.829	-	-
	$1x10^{-5}$	0.289	0.65	65.1
	$5x10^{-5}$	0.253	0.69	69.5
	$1x10^{-4}$	0.228	0.73	72.5
	$5x10^{-4}$	0.230	0.72	72.2
	$1x10^{-3}$	0.172	0.79	79.2

Table (12): Corrosion rate of carbon steel, surface coverage and corrosion inhibition efficiency in absence and presence of different concentrations of E(64) in 1M HCl from gravimetric measurements at various temperatures

Temperature °C	Conc. of inhibitor M	Corrosion Rate mg cm^{-2} h^{-1}	θ	η_w %
30	0.00	0.196	-	-
	$1x10^{-5}$	0.035	0.82	82.1
	$5x10^{-5}$	0.032	0.84	83.6
	$1x10^{-4}$	0.029	0.85	85.3
	$5x10^{-4}$	0.024	0.88	87.6
	$1x10^{-3}$	0.021	0.89	89.4
40	0.00	0.402	-	-
	$1x10^{-5}$	0.128	0.68	68.1
	$5x10^{-5}$	0.094	0.77	76.5
	$1x10^{-4}$	0.083	0.79	79.3
	$5x10^{-4}$	0.072	0.82	82.2
	$1x10^{-3}$	0.063	0.84	84.3
50	0.00	0.829	-	-
	$1x10^{-5}$	0.268	0.68	67.7
	$5x10^{-5}$	0.237	0.71	71.4
	$1x10^{-4}$	0.214	0.74	74.2
	$5x10^{-4}$	0.187	0.77	77.4
	$1x10^{-3}$	0.165	0.80	80.1

Table (13): Corrosion rate of carbon steel, surface coverage and corrosion inhibition efficiency in absence and presence of different concentrations of E(74) in 1M HCl from gravimetric measurements at various temperatures

Temperature °C	Conc. of inhibitor M	Corrosion Rate mg cm^{-2} h^{-1}	θ	η_w %
30	0.00	0.196	-	-
	$1x10^{-5}$	0.032	0.84	83.8
	$5x10^{-5}$	0.029	0.85	85.4
	$1x10^{-4}$	0.024	0.88	87.8
	$5x10^{-4}$	0.019	0.90	90.1
	$1x10^{-3}$	0.017	0.91	91.4
40	0.00	0.402	-	-
	$1x10^{-5}$	0.105	0.74	73.9
	$5x10^{-5}$	0.079	0.80	80.4
	$1x10^{-4}$	0.064	0.84	84.1
	$5x10^{-4}$	0.057	0.86	85.9
	$1x10^{-3}$	0.047	0.88	88.3
50	0.00	0.829	-	-
	$1x10^{-5}$	0.246	0.70	70.3
	$5x10^{-5}$	0.23	0.72	72.2
	$1x10^{-4}$	0.205	0.75	75.3
	$5x10^{-4}$	0.171	0.79	79.4
	$1x10^{-3}$	0.153	0.82	81.5

Table (14): Corrosion rate of carbon steel, surface coverage and corrosion inhibition efficiency in absence and presence of different concentrations of E(84) in 1M HCl from gravimetric measurements at various temperatures

Temperature °C	Conc. of inhibitor M	Corrosion Rate mg cm^{-2} h^{-1}	θ	η_w %
30	0.00	0.196	-	-
	$1x10^{-5}$	0.027	0.86	86.3
	$5x10^{-5}$	0.019	0.90	90.4
	$1x10^{-4}$	0.015	0.92	92.1
	$5x10^{-4}$	0.012	0.94	93.9
	$1x10^{-3}$	0.009	0.95	95.2
40	0.00	0.402	-	-
	$1x10^{-5}$	0.101	0.75	74.8
	$5x10^{-5}$	0.078	0.81	80.6
	$1x10^{-4}$	0.053	0.87	86.9
	$5x10^{-4}$	0.042	0.90	89.5
	$1x10^{-3}$	0.038	0.91	90.5
50	0.00	0.829	-	-
	$1x10^{-5}$	0.213	0.74	74.3
	$5x10^{-5}$	0.191	0.77	77.0
	$1x10^{-4}$	0.162	0.81	80.5
	$5x10^{-4}$	0.148	0.82	82.1
	$1x10^{-3}$	0.128	0.85	84.6

2.7. Potentiodynamic polarization measurements

Tafel polarization plots recorded for carbon steel electrode in 1M HCl in absence and presence of different concentrations of synthesized N,N,N,N-alkyldimethylisopropylammonium bromide, N,N,N,N-alkyldimethyl-isopropylammonium hydroxide or ethoxylated N,N,N,N-dodecyldimethyl-ammonium bromide benzoic acid with 54, 64, 74, 84 units are shown in **Figs. (32–41).**

The corrosion inhibition efficiency (η_p%) and surface coverage (θ) of steel corrosion were calculated using the following equations [110,111]:

$$\eta_p\ \% = [\{i_{corr} - i_{corr}(inh)\}/i_{corr}]\ \text{x}\ 100 \qquad (14)$$

$$\theta = \{i_{corr} - i_{corr}(inh)\}/i_{corr} \qquad (15)$$

where $i_{corr}(inh)$ and i_{corr} are the corrosion current density values with and without inhibitor respectively, which are determined by extrapolation of the cathodic and anodic Tafel slopes to the respective free corrosion potential.

The values of the corrosion current densities (i_{corr}), the corrosion potentials (E_{corr}), the anodic Tafel slopes (βa), the cathodic Tafel slopes (βc), corrosion rate (k), surface coverage (θ) and the percentage of corrosion inhibition efficiencies (η_p%) obtained are given in **Tables (15 -17).**

From results, all prepared surfactants shift the corrosion potential (E_{corr}) in the cathodic direction and the cathodic Tafel slopes (βc) and anodic Tafel slopes (βa) values are changed when compared with those values obtained in the reference solutions, which confirms that the prepared surfactants act as cathodic inhibitor. The data show that the corrosion current density (i_{corr}) values decrease with increasing the concentration of surfactant. Since the corrosion current density is directly related to the corrosion rate (k), the corrosion inhibition efficiency of this compound depends on its concentration. The inhibitive action of this compound is discussed in terms

of blocking the electrode surface by adsorption of the molecules through the active centers contained in its structure.

The model of an electrical double layer with specifically adsorbed N,N,N,N-alkyldimethylisopropylammonium bromide and N,N,N,N-alkyldimethylisopropylammonium hydroxide on carbon steel surface are shown in **Figs. (42, 43)**.

The results are obtained from the gravimetric measurements which are in good agreement with those obtained from potentiodynamic polarization method. Gravimetric and polarization curves measurements are repeated several times and it is observed that they are highly reproducible.

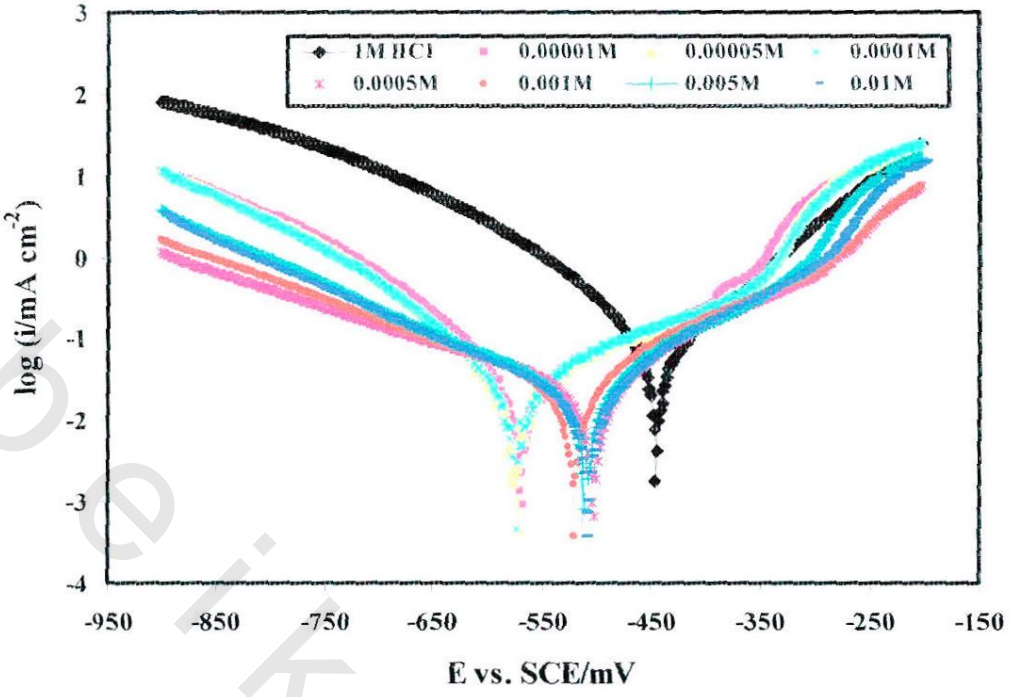

Fig. (32): Polarization curves of carbon steel in 1M HCl in absence and presence of different concentrations of DEDIABr.

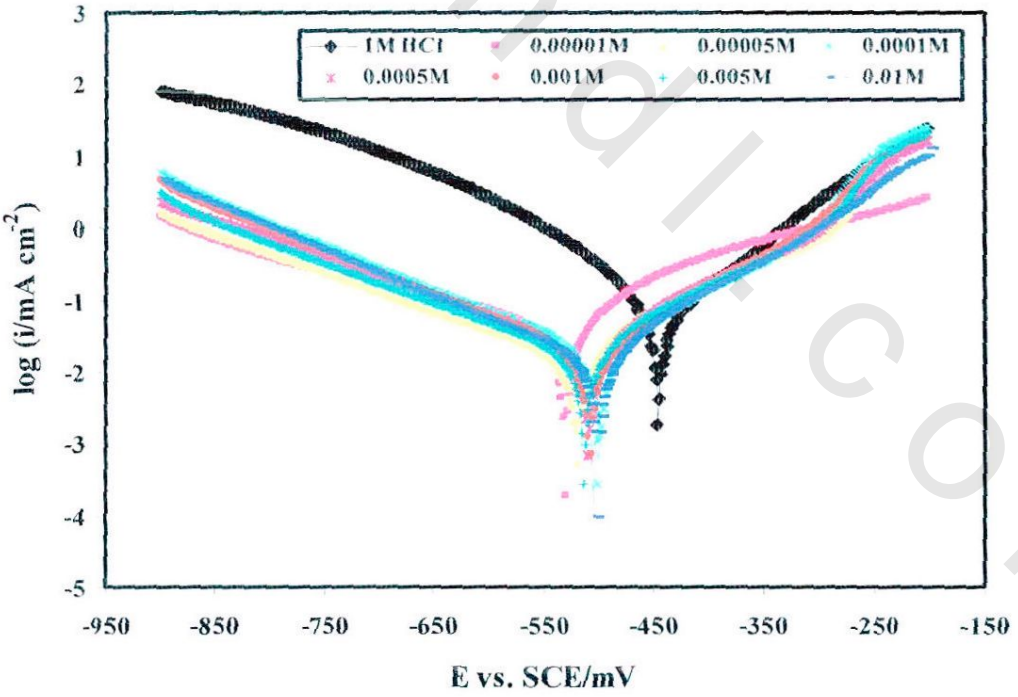

Fig. (33): Polarization curves of carbon steel in 1M HCl in absence and presence of different concentrations of DODIABr.

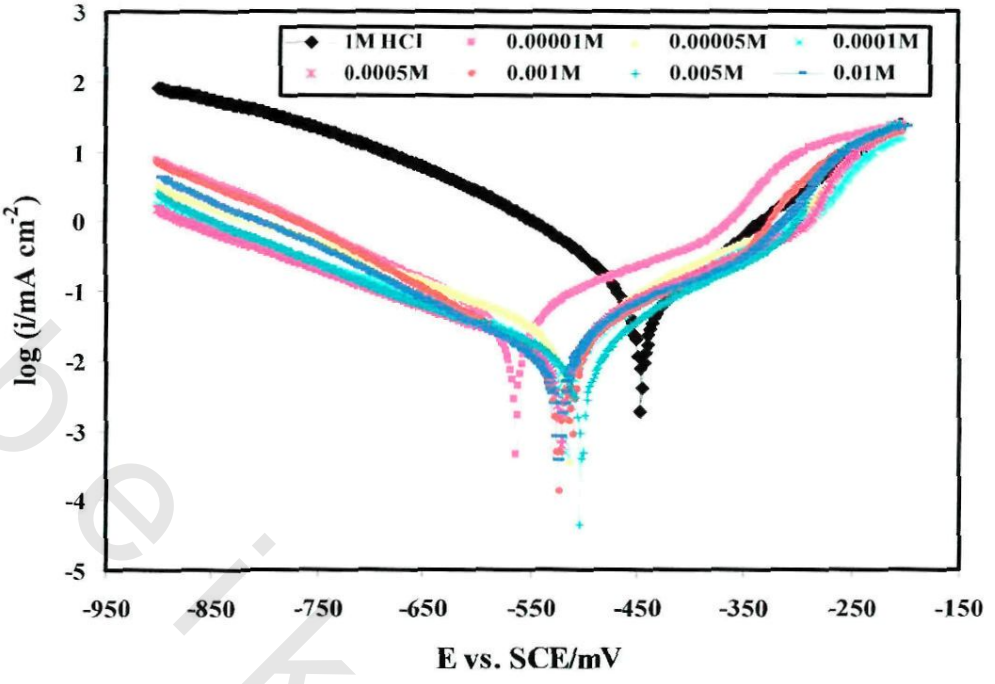

Fig. (34): Polarization curves of carbon steel in 1M HCl in absence and presence of different concentrations of HEDIBr.

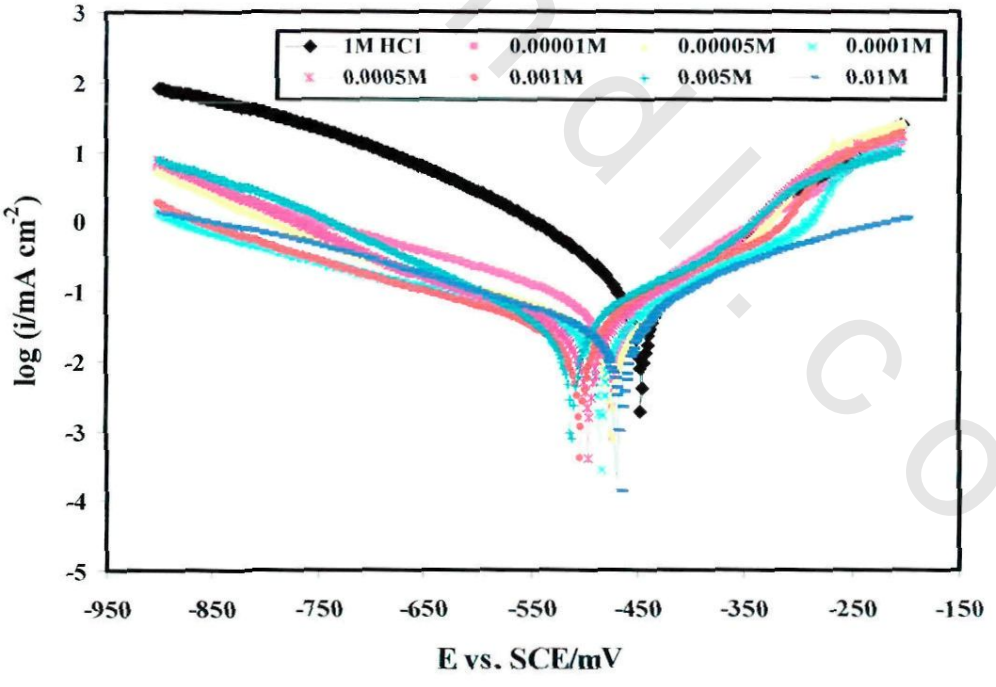

Fig. (35): Polarization curves of carbon steel in 1M HCl in absence and presence of different concentrations of DEDIAOH.

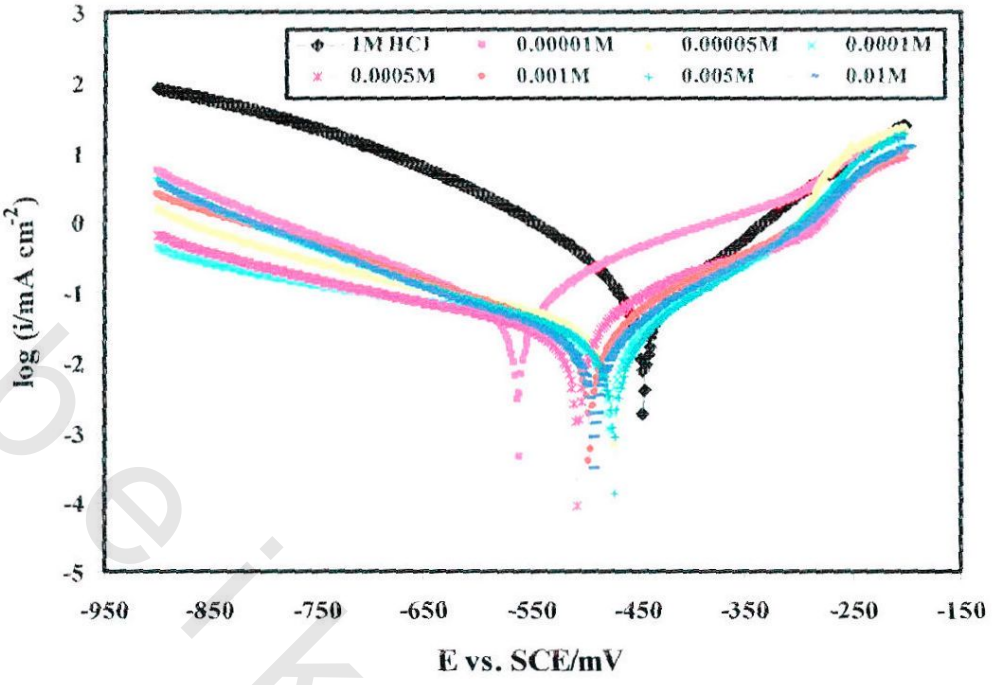

Fig. (36): Polarization curves of carbon steel in 1M HCl in absence and presence of different concentrations of DODIAOH.

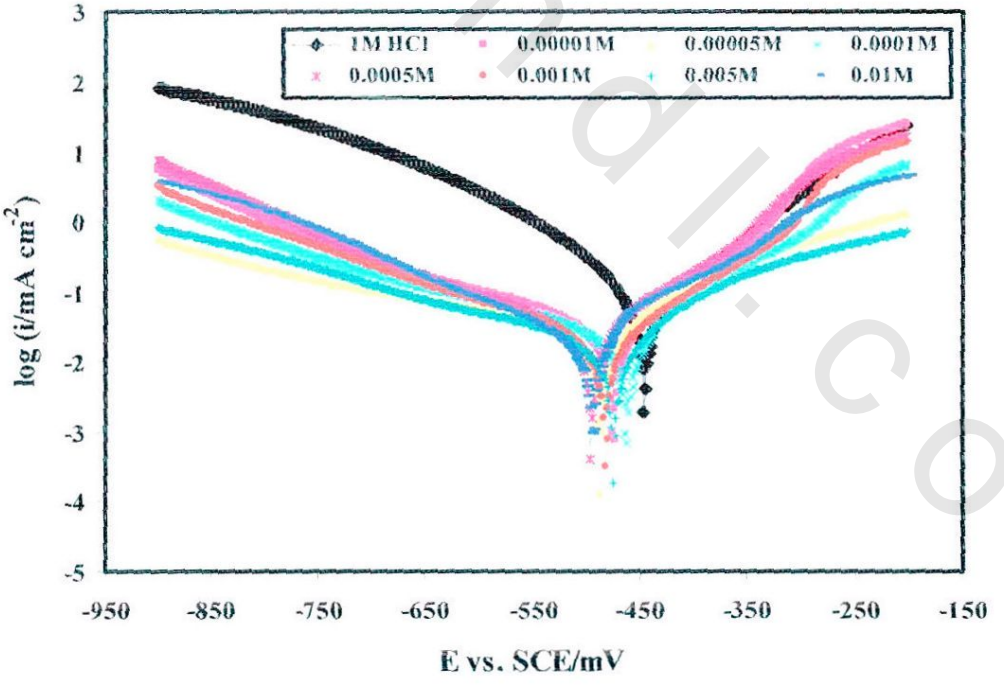

Fig. (37): Polarization curves of carbon steel in 1M HCl in absence and presence of different concentrations of HEDIAOH.

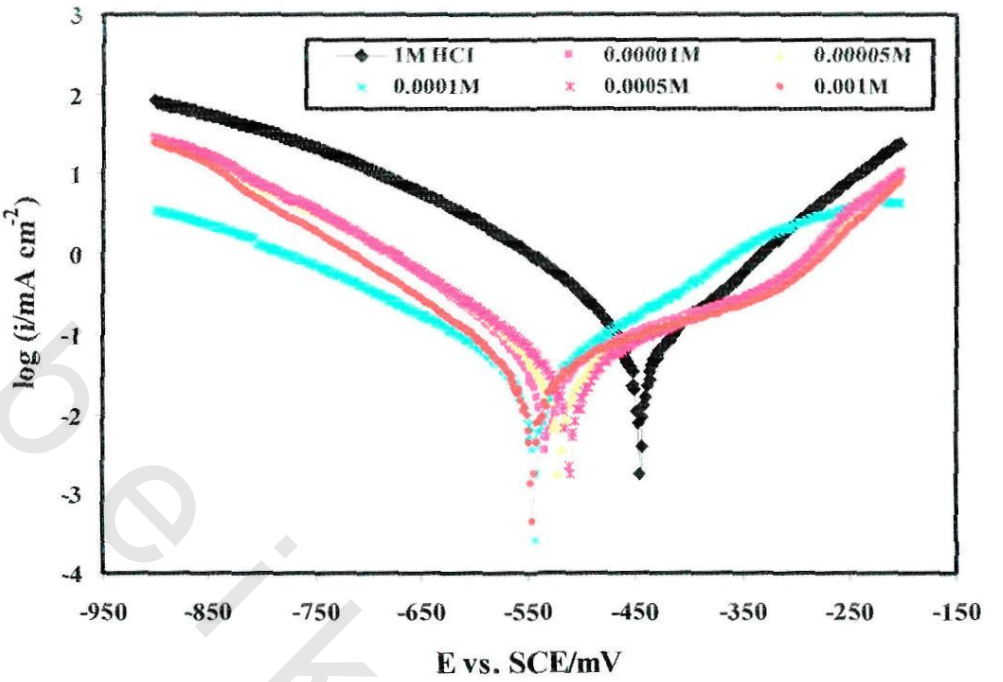

Fig. (38): Polarization curves of carbon steel in 1M HCl in absence and presence of different concentrations of E(54).

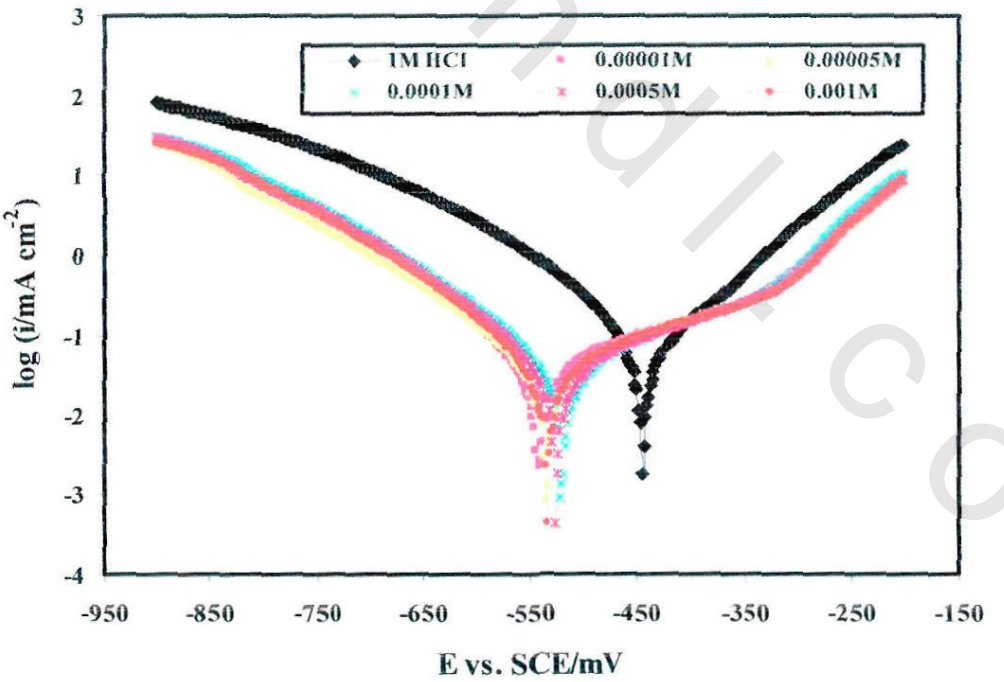

Fig. (39): Polarization curves of carbon steel in 1M HCl in absence and presence of different concentrations of E(64).

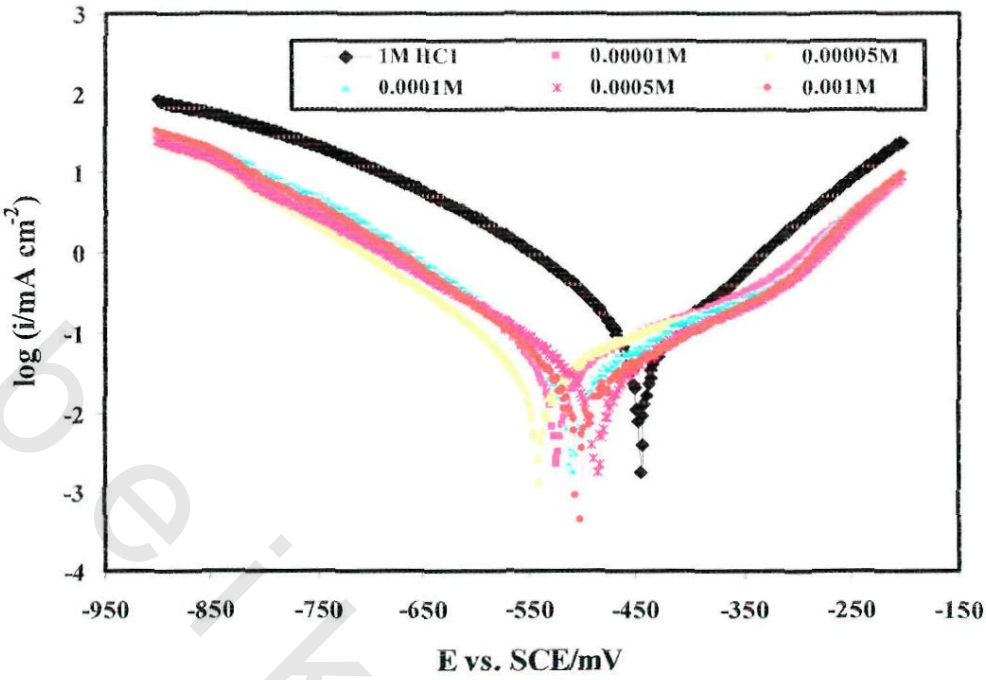

Fig. (40): Polarization curves of carbon steel in 1M HCl in absence and presence of different concentrations of E(74).

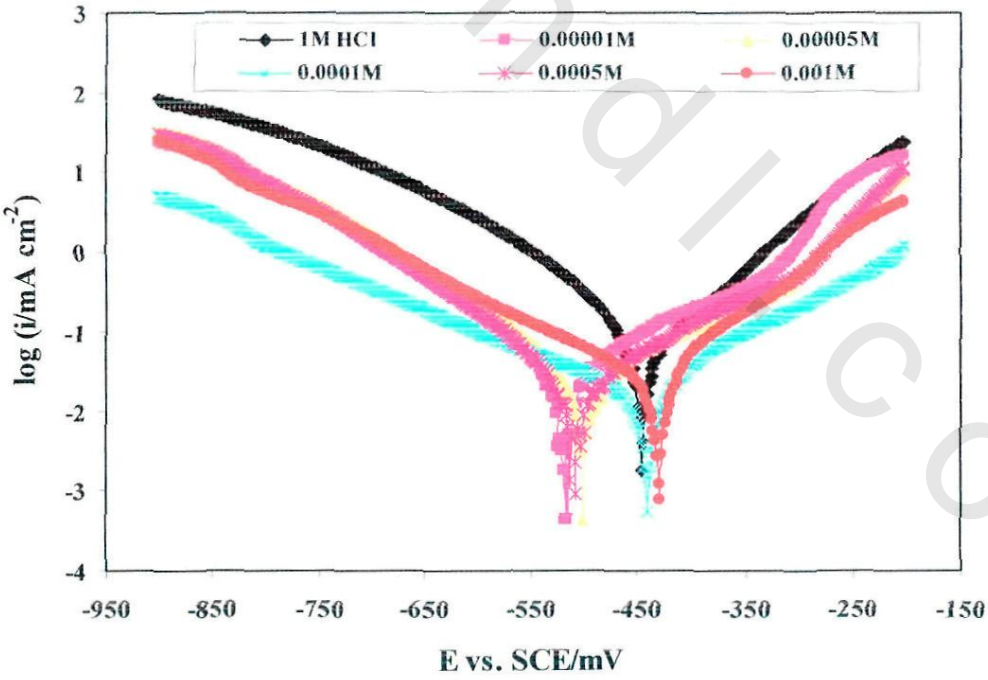

Fig. (41): Polarization curves of carbon steel in 1M HCl in absence and presence of different concentrations of E(84).

Table (15): Potentiodynamic polarization results of carbon steel in absence and presence of different concentrations of the synthesized N,N,N,N-alkyldimethylisopropylammonium bromide in 1M HCl at 30 °C

Inhibitor name	Conc. of inhibitor M	E_{corr} mV	i_{corr} mA cm^{-2}	βa mV dec^{-1}	βc mV dec^{-1}	θ	η_p %
Absence	0.00	-447.3	0.2271	126.1	-143.4	-	-
DEDIABr	$1x10^{-5}$	-570.7	0.0452	250.4	-113.1	0.80	80.10
	$5x10^{-5}$	-576.4	0.0343	222.4	-107.4	0.85	84.90
	$1x10^{-4}$	-575.9	0.0314	203.0	-105.1	0.86	86.17
	$5x10^{-4}$	-504.2	0.0222	122.8	-247.3	0.90	90.22
	$1x10^{-3}$	-521.8	0.0211	119.9	-202.1	0.91	90.71
	$5x10^{-3}$	-511.5	0.0177	126.4	-175.1	0.92	92.21
	$1x10^{-2}$	-513.9	0.0151	103.3	-168.3	0.93	93.35
DODIABr	$1x10^{-5}$	-508.9	0.0409	116.4	-287.9	0.82	81.99
	$5x10^{-5}$	-521.4	0.0279	161.8	-260.7	0.88	87.71
	$1x10^{-4}$	-502.0	0.0196	119.6	-184.7	0.91	91.37
	$5x10^{-4}$	-511.9	0.0175	102.9	-173.1	0.92	92.29
	$1x10^{-3}$	-509.3	0.0166	114.0	-166.6	0.93	92.69
	$5x10^{-3}$	-515.1	0.0157	120.7	-179.9	0.93	93.09
	$1x10^{-2}$	-506.7	0.0121	105.1	-154.0	0.95	94.67
HEDIABr	$1x10^{-5}$	-468.2	0.0368	106.0	-222.2	0.84	83.80
	$5x10^{-5}$	-515.6	0.0216	107.3	-171.4	0.90	90.49
	$1x10^{-4}$	-519.1	0.0147	110.1	-190.2	0.94	93.53
	$5x10^{-4}$	-522.3	0.0111	119.3	-180.3	0.95	95.11
	$1x10^{-3}$	-522.3	0.0094	112.4	-120.4	0.96	95.86
	$5x10^{-3}$	-504.3	0.0090	108.0	-176.5	0.96	96.04
	$1x10^{-2}$	-529.2	0.0087	113.2	-132.4	0.96	96.17

Table (16): Potentiodynamic polarization results of carbon steel in absence and presence of different concentrations of the synthesized N,N,N,N-alkyldimethylisopropylammonium hydroxide in 1M HCl at 30 °C

Inhibitor name	Conc. of inhibitor M	E_{corr} mV	i_{corr} mA cm^{-2}	βa mV dec^{-1}	βc mV dec^{-1}	θ	η_p %
Absence	0.00	-447.3	0.2271	126.1	-143.4	-	-
DEDIAOH	$1x10^{-5}$	-474.0	0.0646	118.0	-237.4	0.72	71.55
	$5x10^{-5}$	-475.5	0.0345	114.8	-261.6	0.85	84.81
	$1x10^{-4}$	-485.4	0.0299	137.2	-294.2	0.87	86.83
	$5x10^{-4}$	-497.2	0.0280	117.6	-204.2	0.88	87.67
	$1x10^{-3}$	-504.7	0.0243	128.1	-240.3	0.89	89.30
	$5x10^{-3}$	-513.2	0.0226	113.9	-137.5	0.90	90.05
	$1x10^{-2}$	-471.0	0.0216	94.60	-207.1	0.90	90.49
DODIAOH	$1x10^{-5}$	-563.6	0.0530	116.5	-176.3	0.77	76.66
	$5x10^{-5}$	-475.7	0.0315	128.2	-312.7	0.86	86.13
	$1x10^{-4}$	-478.8	0.0277	127.6	-306.3	0.88	87.80
	$5x10^{-4}$	-509.6	0.0244	108.8	-310.1	0.89	89.26
	$1x10^{-3}$	-496.9	0.0233	125.8	-196.5	0.90	89.74
	$5x10^{-3}$	-474.9	0.0202	112.7	-231.5	0.91	91.11
	$1x10^{-2}$	-497.7	0.0183	119.7	-205.4	0.92	91.94
HEDIAOH	$1x10^{-5}$	-475.5	0.0345	114.8	-261.6	0.85	84.81
	$5x10^{-5}$	-488.6	0.0283	132.4	-275.4	0.88	87.54
	$1x10^{-4}$	-463.5	0.0252	115.7	-283.2	0.89	88.90
	$5x10^{-4}$	-467.7	0.0204	72.00	-187.0	0.91	91.02
	$1x10^{-3}$	-483.4	0.0168	105.5	-190.2	0.93	92.60
	$5x10^{-3}$	-475.8	0.0161	110.1	-260.9	0.93	92.91
	$1x10^{-2}$	-500.1	0.0137	100.7	-144.8	0.94	93.97

Table (17): Potentiodynamic polarization results of carbon steel in absence and presence of different concentrations of the synthesized ethoxylated N,N,N,N-dodecyldimethylammonium bromide benzoic acid with 54, 64, 74, 84 units in 1M HCl at 30 °C

Inhibitor name	Conc. of inhibitor M	E_{corr} mV	i_{corr} mA cm^{-2}	βa mV dec^{-1}	βc mV dec^{-1}	θ	η_p %
Absence	0.00	-367.3	0.2271	126.1	-143.4	-	-
E(54)	$1x10^{-5}$	-533.2	0.0481	238.3	-109.8	0.78	78.3
	$5x10^{-5}$	-522.0	0.0425	209.1	-110.6	0.83	82.6
	$1x10^{-4}$	-545.3	0.0402	146.5	-162.1	0.84	84.5
	$5x10^{-4}$	-512.2	0.0378	184.6	-115.1	0.86	85.9
	$1x10^{-3}$	-546.3	0.0366	246.7	-117.8	0.88	88.4
E(64)	$1x10^{-5}$	-543.6	0.0433	257.0	-104.8	0.82	82.1
	$5x10^{-5}$	-536.8	0.0423	231.3	-114.1	0.84	83.6
	$1x10^{-4}$	-521.8	0.0402	209.8	-107.0	0.85	85.3
	$5x10^{-4}$	-527.6	0.0377	211.4	-102.9	0.88	87.6
	$1x10^{-3}$	-534.9	0.0362	226.0	-98.70	0.89	89.4
E(74)	$1x10^{-5}$	-532.0	0.0417	226.8	-98.60	0.84	83.8
	$5x10^{-5}$	-543.4	0.0387	243.5	-115.3	0.85	85.4
	$1x10^{-4}$	-511.2	0.0347	186.6	-105.9	0.88	87.8
	$5x10^{-4}$	-488.6	0.0305	165.7	-131.6	0.90	90.1
	$1x10^{-3}$	-504.9	0.0280	173.1	-108.6	0.91	91.4
E(84)	$1x10^{-5}$	-519.6	0.0368	172.2	-116.2	0.86	86.3
	$5x10^{-5}$	-502.6	0.0300	179.5	-112.1	0.90	90.4
	$1x10^{-4}$	-521.4	0.0279	161.8	-260.7	0.92	92.1
	$5x10^{-4}$	-510.3	0.0255	151.8	-108.0	0.94	93.9
	$1x10^{-3}$	-510.7	0.0164	86.0	-139.6	0.95	95.2

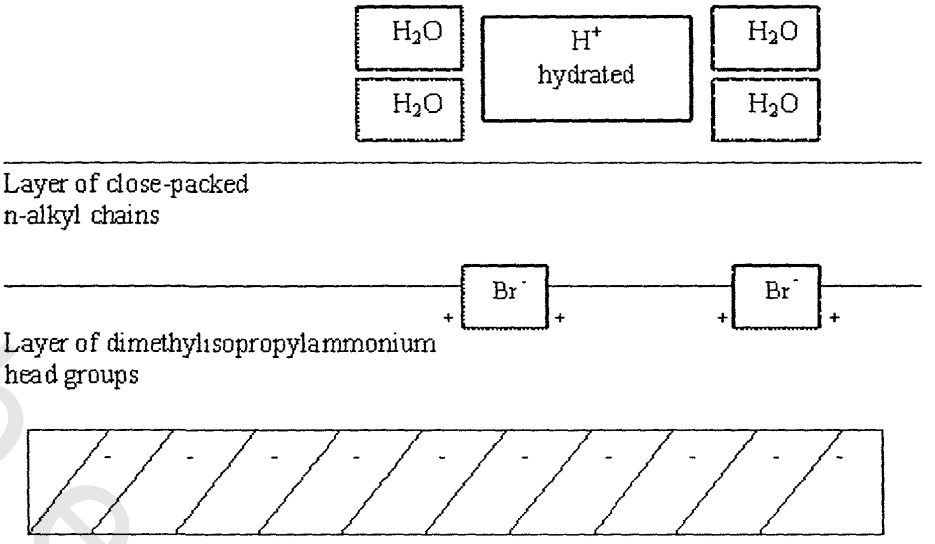

Fig. (42): Electrical double layer of n-alkyldimethylisopropylammonium bromide adsorbed on carbon steel surface.

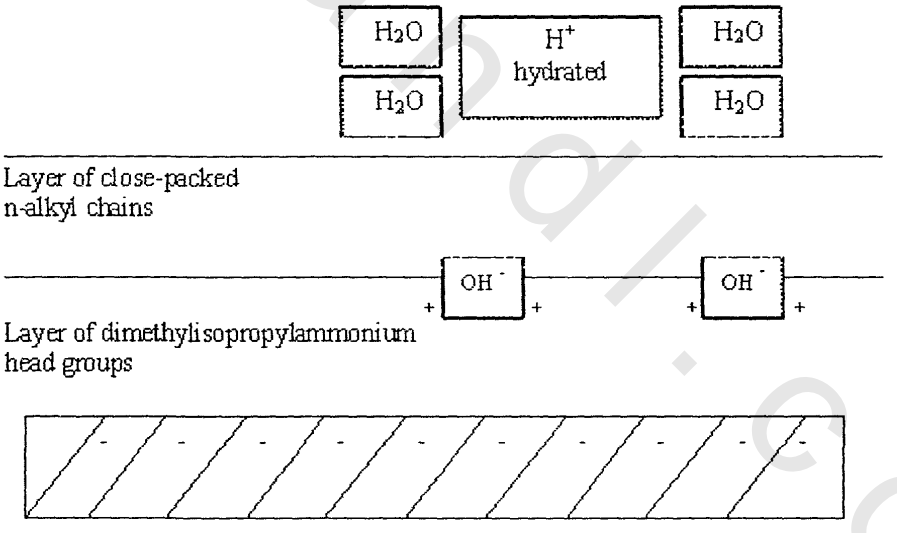

Fig. (43): Electrical double layer of n-alkyldimethylisopropylammonium hydroxide adsorbed on carbon steel surface.

2.8. Corrosion inhibition mechanism

Gravimetric measurements were performed in the temperature range from 30 to 50 °C in absence or presence of different concentrations for N,N,N,N-alkyldimethylisoprpylammonium bromide, N,N,N,N-alkyl-dimethylisoprpylammonium hydroxide and ethoxylated N,N,N,N-dodecyl-dimethylammonium bromide benzoic acid with 54, 64, 74 and 84 units. The corrosion inhibition efficiencies were calculated and listed in **Tables (5-14)**. Inspection of these tables reveals that as the temperature increases a decrease in η_w %, which indicates the formation of an adsorptive film, has a physical character. The dependence of corrosion rate on temperature can be expressed by the Arrhenius equation [112, 113]:

$$k = A \exp(-E_a / RT) \qquad (10)$$

where k is the corrosion rate, A is Arrhenius constant, E_a is the activation energy of the metal dissolution reaction, R is the gas constant and T is the absolute temperature.

The E_a values can be determined from the slopes of Arrhenius plots (log k versus 1/T) as shown in **Figs. (44-53)**. The E_a values in absence and presence of different concentrations of the prepared surfactants in 1M HCl in the temperature range from 30 to 50 °C are listed in **Tables (18-20)**. It was found that, the increase in activation energy in presence of corrosion inhibitor indicates that physical adsorption (electrostatic) occurs in the first stage [114]. On the other hand, the adsorption phenomenon of an organic molecule is not considered only as a physical or as a chemical adsorption phenomenon. A wide spectrum of conditions, ranging from the dominance of chemisorption or electrostatic effects arises from other adsorption experimental data [115].

Data in **Tables (18-20)** reveals that, E_a values in absence of corrosion inhibitors are less than in presence of prepared corrosion inhibitors,

indicating formation of corrosion inhibitors layer at the metal surface. Data shows that, E_a values are increased by increasing the concentration of prepared corrosion inhibitors. It is obvious that concentration of inhibitors play an important role in increasing the activation energy value, thereby indicating a more efficient inhibiting effect. The increase in the activation energy, E_a, can correlate to the thickening of the electrical double layer (116).

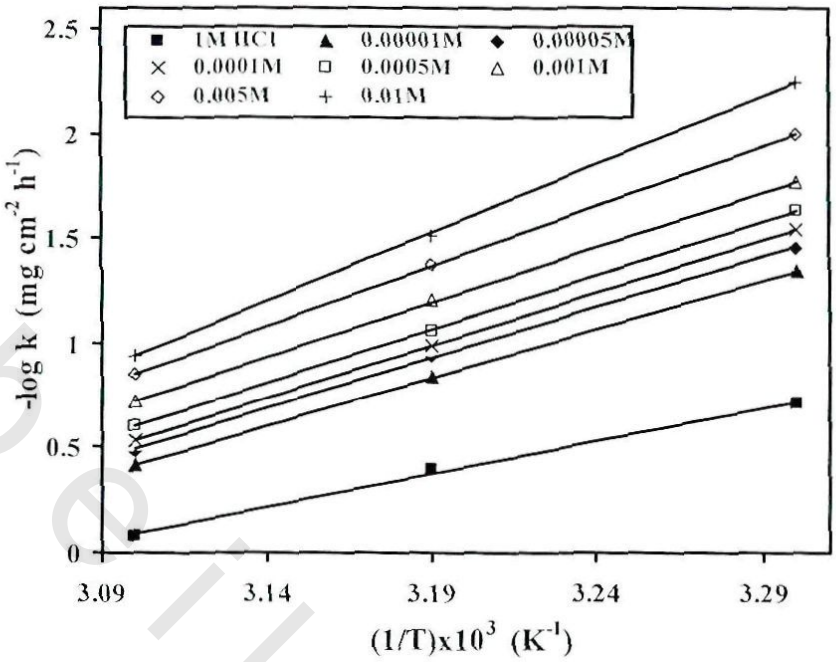

Fig. (44): Arrhenius plots of the corrosion rate for carbon steel in 1M HCl in absence and presence of different concentrations of DEDIABr at 30, 40 and 50 °C.

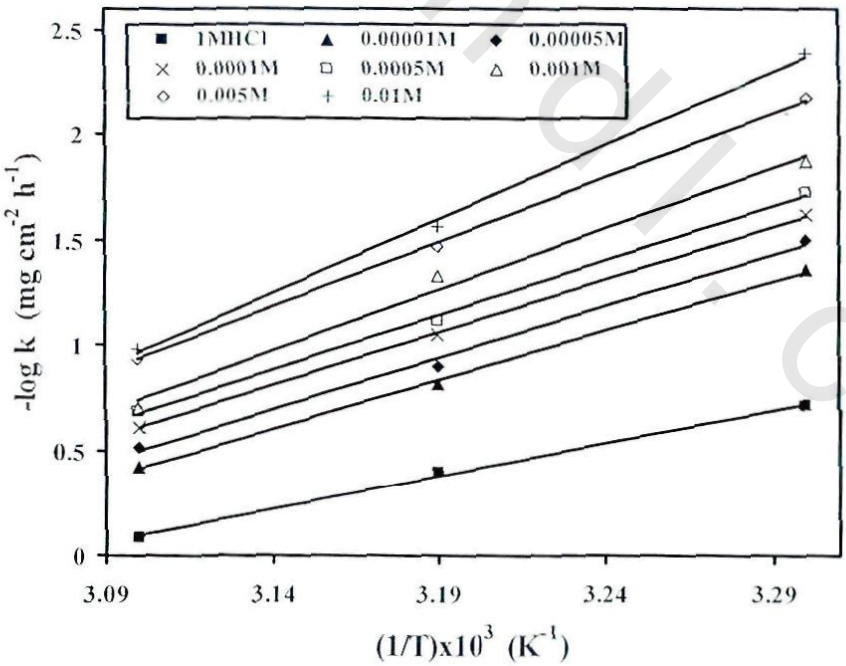

Fig. (45): Arrhenius plots of the corrosion rate for carbon steel in 1M HCl in absence and presence of different concentrations of DODIABr at 30, 40 and 50 °C.

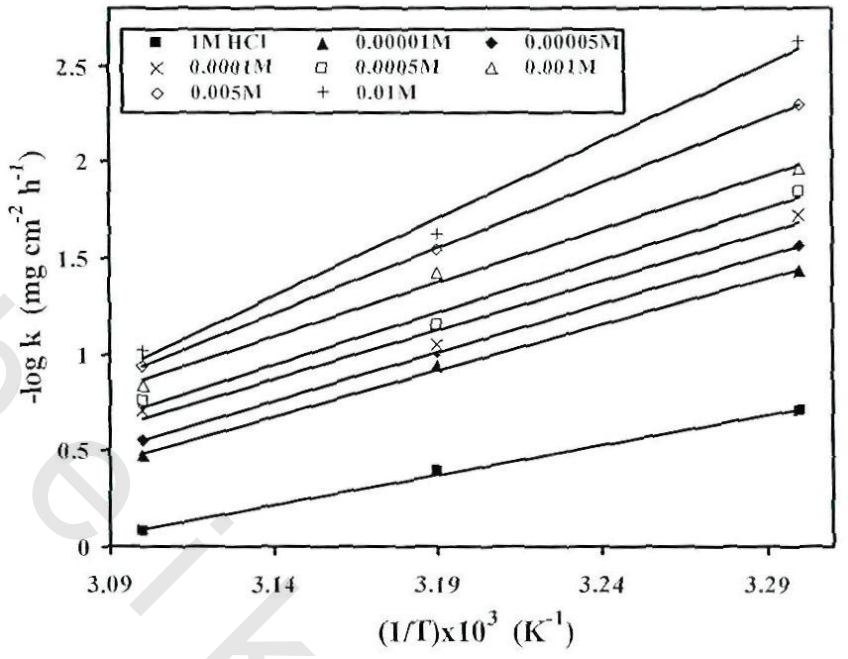

Fig. (46): Arrhenius plots of the corrosion rate for carbon steel in 1M HCl in absence and presence of different concentrations of HEDIABr at 30, 40 and 50 °C.

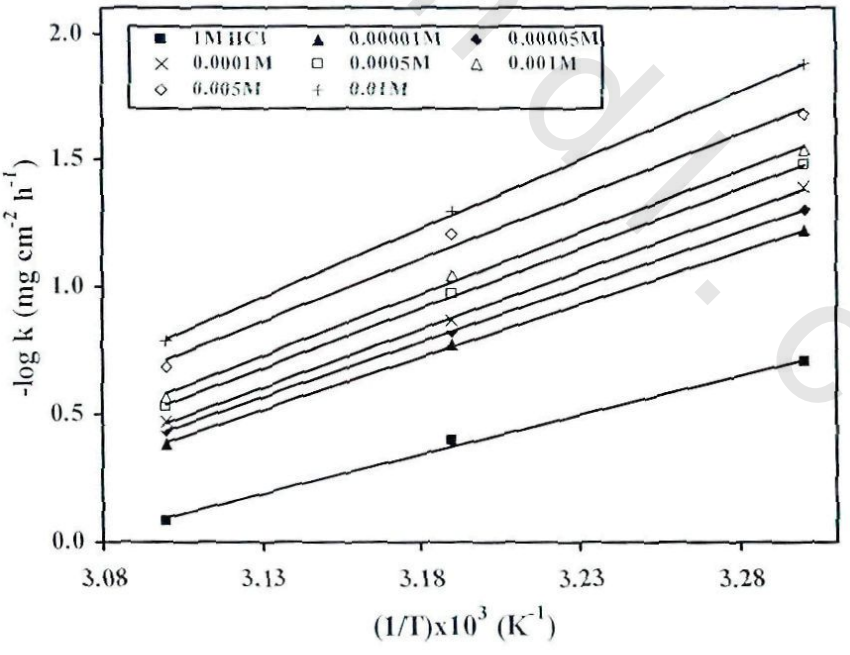

Fig. (47): Arrhenius plots of the corrosion rate for carbon steel in 1M HCl in absence and presence of different concentrations of DEDIAOH at 30, 40 and 50 °C.

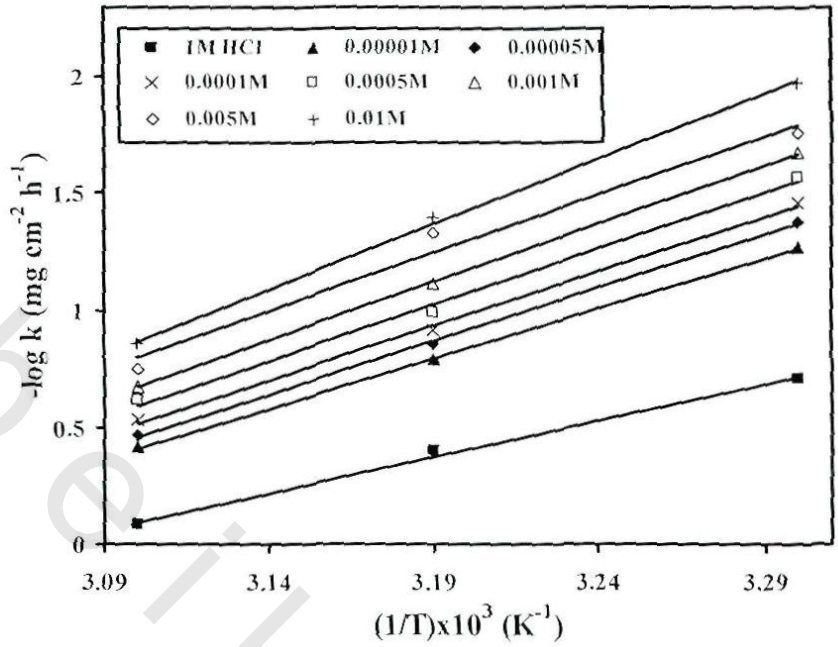

Fig. (48): Arrhenius plots of the corrosion rate for carbon steel in 1M HCl in absence and presence of different concentrations of DODIAOH at 30, 40 and 50 °C.

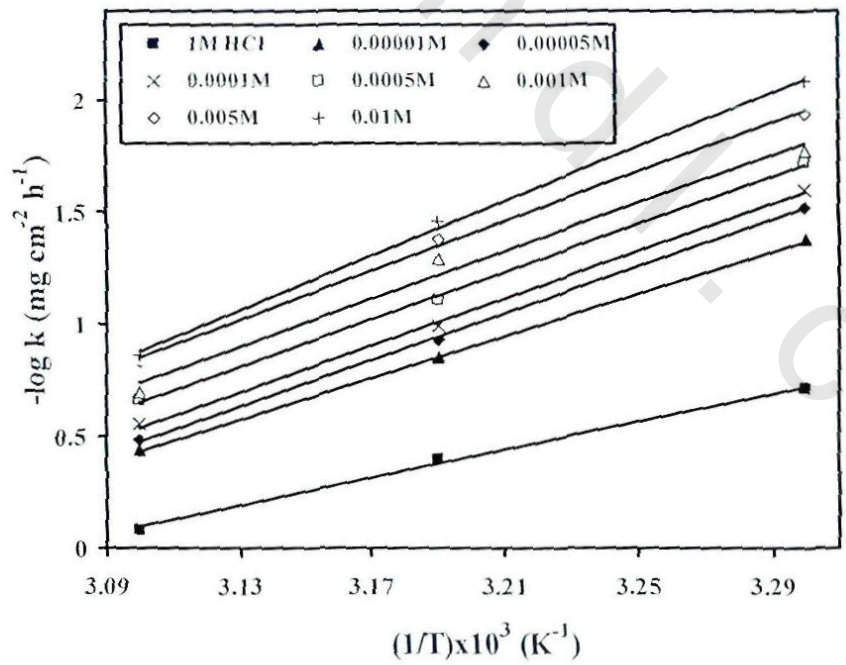

Fig. (49): Arrhenius plots of the corrosion rate for carbon steel in 1M HCl in absence and presence of different concentrations of HEDIAOH at 30, 40 and 50 °C.

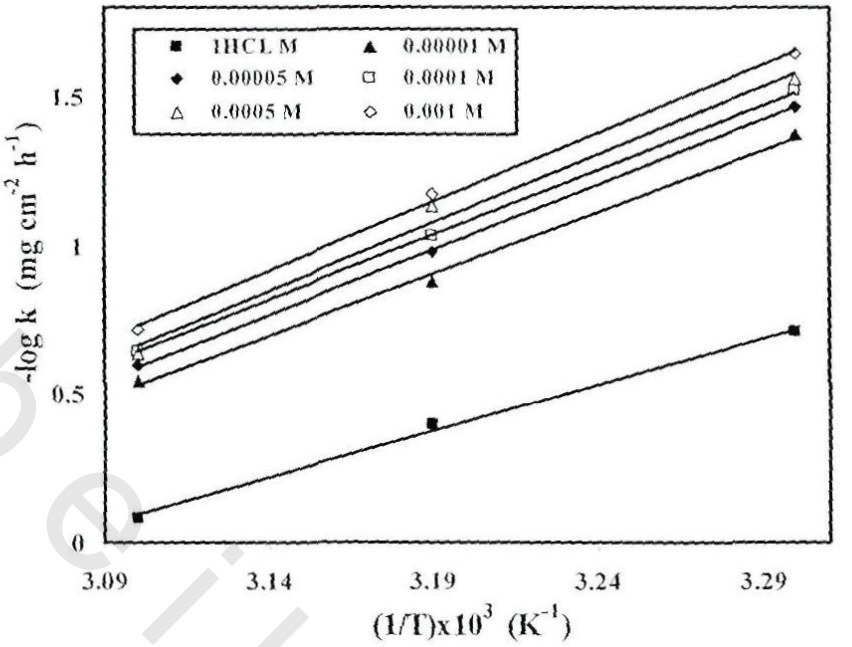

Fig. (50): Arrhenius plots of the corrosion rate for carbon steel in 1M HCl in absence and presence of different concentrations of E(54) at 30, 40 and 50 °C.

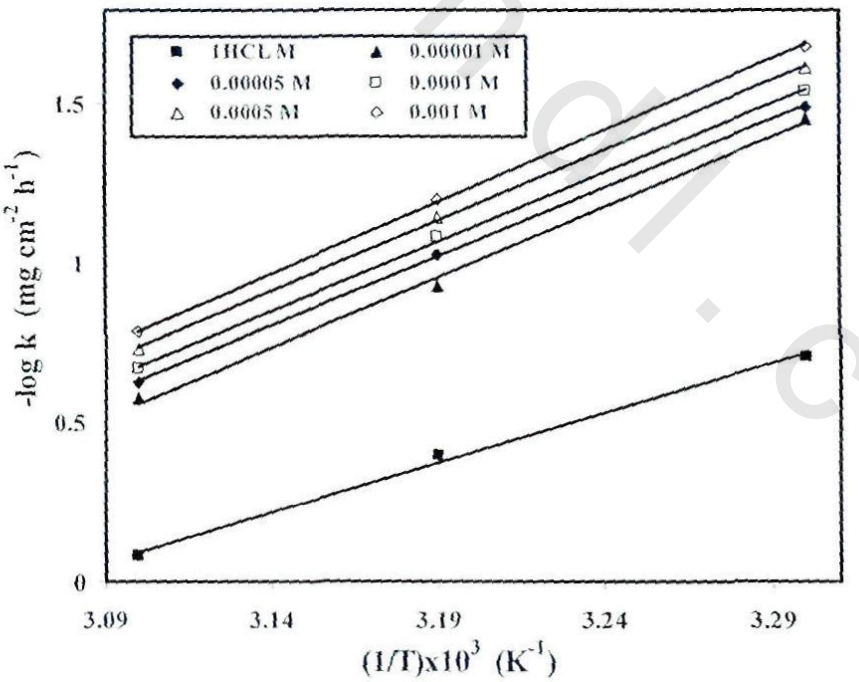

Fig. (51): Arrhenius plots of the corrosion rate for carbon steel in 1M HCl in absence and presence of different concentrations of E(64) at 30, 40 and 50 °C.

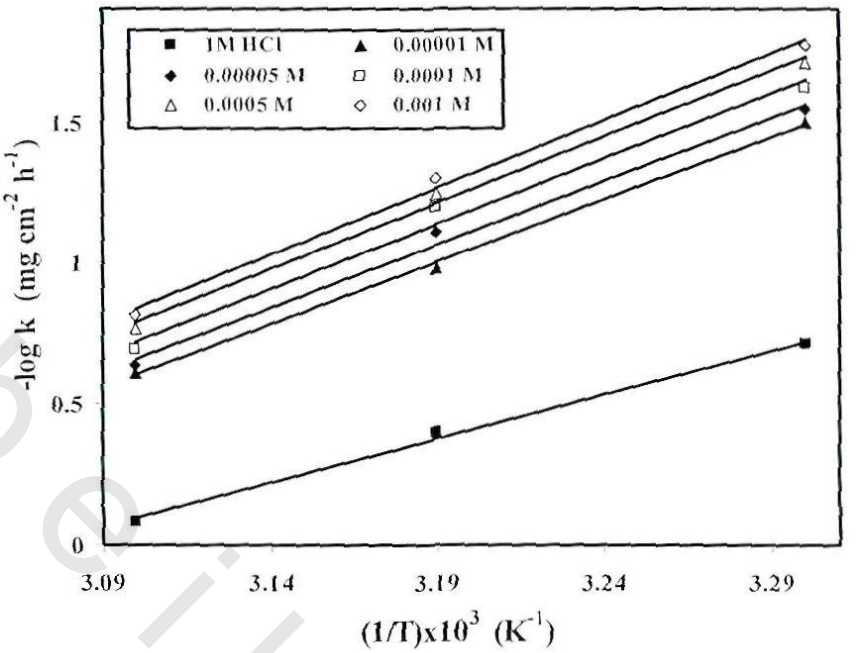

Fig. (52): Arrhenius plots of the corrosion rate for carbon steel in 1M HCl in absence and presence of different concentrations of E(74) at 30, 40 and 50 °C.

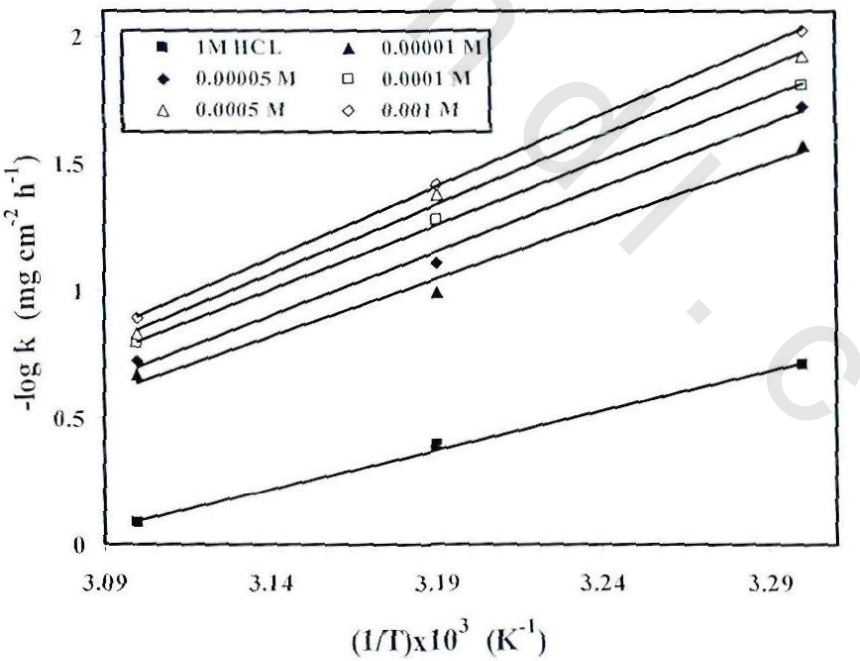

Fig. (53): Arrhenius plots of the corrosion rate for carbon steel in 1M HCl in absence and presence of different concentrations of E(84) at 30, 40 and 50 °C.

Table (18): Activation energy values of carbon steel in absence and presence of different concentrations of the synthesized N,N,N,N-alkyl-dimethylisopropylammonium bromide in 1M HCl at 30, 40 and 50 °C

Inhibitor name	Inhibitor Conc. M	E_a kJ mol^{-1}
Absence	0.00	59.70
DEDIABr	$1x10^{-5}$	88.88
	$5x10^{-5}$	93.06
	$1x10^{-4}$	96.17
	$5x10^{-4}$	98.62
	$1x10^{-3}$	100.0
	$5x10^{-3}$	109.7
	$1x10^{-2}$	124.3
DODIABr	$1x10^{-5}$	89.39
	$5x10^{-5}$	93.81
	$1x10^{-4}$	96.42
	$5x10^{-4}$	99.92
	$1x10^{-3}$	110.7
	$5x10^{-3}$	117.9
	$1x10^{-2}$	134.4
HEDIABr	$1x10^{-5}$	91.75
	$5x10^{-5}$	96.34
	$1x10^{-4}$	97.79
	$5x10^{-4}$	104.1
	$1x10^{-3}$	107.8
	$5x10^{-3}$	129.6
	$1x10^{-2}$	155.0

Table (19): Activation energy values of carbon steel in absence and presence of different concentrations of the synthesized N,N,N,N-alkyldimethylisopropylammonium hydroxide in 1M HCl at 30, 40 and 50 °C

Inhibitor name	Inhibitor Conc. M	E_a kJ mol^{-1}
Absence	0.00	59.70
DEDIAOH	$1x10^{-5}$	80.14
	$5x10^{-5}$	83.14
	$1x10^{-4}$	88.34
	$5x10^{-4}$	90.78
	$1x10^{-3}$	92.74
	$5x10^{-3}$	94.88
	$1x10^{-2}$	104.1
DODIAOH	$1x10^{-5}$	81.92
	$5x10^{-5}$	87.83
	$1x10^{-4}$	88.85
	$5x10^{-4}$	92.35
	$1x10^{-3}$	95.69
	$5x10^{-3}$	95.91
	$1x10^{-2}$	107.5
HEDIAOH	$1x10^{-5}$	89.85
	$5x10^{-5}$	99.48
	$1x10^{-4}$	100.4
	$5x10^{-4}$	101.4
	$1x10^{-3}$	102.5
	$5x10^{-3}$	105.8
	$1x10^{-2}$	116.9

Table (20): Activation energy values of carbon steel in absence and presence of different concentrations of the synthesized ethoxylated N,N,N,N-dodecyldimethylammonium bromide benzoic acid in 1M HCl at 30, 40 and 50 °C

°

Inhibitor name	Conc. of inhibitor M	E_a kJ mol^{-1}
Absence	0.00	59.70
E(54)	$1x10^{-5}$	79.88
	$5x10^{-5}$	83.38
	$1x10^{-4}$	83.68
	$5x10^{-4}$	87.77
	$1x10^{-3}$	88.51
E(64)	$1x10^{-5}$	84.94
	$5x10^{-5}$	86.12
	$1x10^{-4}$	87.77
	$5x10^{-4}$	89.13
	$1x10^{-3}$	92.88
E(74)	$1x10^{-5}$	85.30
	$5x10^{-5}$	86.33
	$1x10^{-4}$	88.71
	$5x10^{-4}$	90.03
	$1x10^{-3}$	93.51
E(84)	$1x10^{-5}$	86.6
	$5x10^{-5}$	96.64
	$1x10^{-4}$	99.21
	$5x10^{-4}$	104.3
	$1x10^{-3}$	108.3

2.9. Adsorption isotherm and thermodynamic consideration

Adsorption on corroding surfaces never reaches the real equilibrium and tends to an adsorption steady state. However, when the corrosion rate is sufficiently small, the adsorption steady state has a tendency to become a quasi-equilibrium state. In this case, it is reasonable to consider the quasi-equilibrium adsorption in thermodynamic way using the appropriate equilibrium isotherms [117]. The adsorption isotherms can provide basic information on the interaction of inhibitor and metal surface.

In order to obtain adsorption isotherm, the surface coverage values (θ), for different concentrations of N,N,N,N-alkyldimethylisopropylammonium bromide, N,N,N,N-alkyldimethylisopropylammonium hydroxide and ethoxylted N,N,N,N-dodecyldimethylammonium bromide benzoic acid with 54, 64, 74, 84 units in 1M HCl solution have been obtained from gravimetric measurements and tested graphically for fitting a suitable adsorption isotherm. The plots of C/θ versus C for the prepared surfactants are shown in **Figs. (54-63)** which shows a straight line with correlation coefficient of 0.9998 and the slope closed to 1 providing that the adsorption of the prepared surfactants in hydrochloric acid solution on the carbon steel surface obeys Langmiur adsorption isotherm, presented by Eq. (11).

$$C/\theta = 1/K_{ads} + C \qquad (11)$$

where C is the inhibitor concentration, θ is the degree of surface coverage on the metal surface and K_{ads} is the equilibrium constant for adsorption desorption process.

The values of equilibrium constants, K_{ads}, for all prepared surfactants are calculated from the reciprocal of the intercept of isotherm line at various temperatures 30, 40 and 50 °C listed in **Table (21, 22)**.

For cationic surfactants, it is obvious that the value of equilibrium constant decrease with increasing temperature, indicating that the adsorption type of the prepared inhibitors on the steel surface is physical adsorption. The high values of the adsorption equilibrium constant $2.5x10^4$, $3.33x10^4$ and $5.00x10^4$ M^{-1} for DEDIABr, DODIABr and HEDIABr, respectively at 30 °C, while the values of equilibrium constant are $2x10^4$, $2.5x10^4$ and $3.33x10^4$ M^{-1} for DEDIAOH, DODIAOH and HEDIAOH, respectively at 30 °C, which reflect the high adsorption ability of the latter inhibitors on carbon steel surface. The free energy of adsorption of corrosion inhibitor on carbon steel surface can be evaluated with the following equation [118, 119]:

$$\Delta G_{ads} = -RT \ln (55.5K_{ads}) \qquad (12)$$

where ΔG_{ads} is the free energy of adsorption process, K_{ads} is the equilibrium constant for adsorption desorption process, R is the gas constant, T is the absolute temperature and 55.5 is the molar concentration of water.

ΔG_{ads} values are calculated and are found to be −35.63, −36.29 and −37.31 kJ mol^{-1} for DEDIABr, DODIABr and HEDIABr, respectively at 30 °C while they are −35.07, −35.63 and −36.29 kJ mol^{-1} for DEDIAOH, DODIAOH and HEDIAOH, respectively at 30 °C. The negative values of ΔG_{ads} indicate spontaneous adsorption of the prepared surfactants on the carbon steel surface [120] and also the strong interaction between inhibitor molecules and metal surface [121]. The absolute values of ΔG_{ads} are less than -40 kJ mol^{-1} indicating the electrostatic interaction between the charged inhibitor molecules and the charged metal surface (physical adsorption) [122-124].

When, ln K_{ads} is plotted against 1/T at different concentrations of the cationic surfactants concentration as shown in **Figs. (64,65)**. The slope of the straight line gives the value of $-\Delta H_{ads}/R$. ΔH_{ads} values are calculated

and are found to be −28.24, −28.09 and −28.19 kJ mol^{-1} for DEDIABr, DODIABr and HEDIABr, respectively while they are found −28.18, −32.98 and −28.09 kJ mol^{-1} for DEDIAOH, DODIAOH and HEDIAOH, respectively. The negative sign of ΔH_{ads} indicates that the adsorption of the prepared surfactants on the carbon steel surface in 1M HCl solution is an exothermic process.

Entropy of inhibitor adsorption (ΔS_{ads}) is calculated using the relation:

$$\mathbf{\Delta G_{ads} = \Delta H_{ads} - T\Delta S_{ads}} \qquad \mathbf{(13)}$$

where, ΔG_{ads} is the free energy of adsorption process, T is the absolute temperature, ΔH_{ads} is the enthalpy and ΔS_{ads} is the entropy of adsorption process.

ΔS_{ads} values are found to be 24.38, 27.06 and 30.09 J mol^{-1} K^{-1} for DEDIABr, DODIABr and HEDIABr, respectively at 30 °C and are found to be 22.72, 8.74 and 27.06 J mol^{-1} K^{-1} for DEDIAOH, DODIAOH and HEDIAOH, respectively at 30 °C. The positive value of ΔS_{ads} is attributed to the increase of disorder due to the adsorption of only one surfactant molecule by desorption of more water molecules [125].

For ethoxylated-cationic surfactants, the values of equilibrium constant are $1.67x10^5$, $2.00x10^5$, $2.50x10^5$ and $3.33x10^5$ M^{-1} for ethoxylted N,N,N,N-dodecyldimethylammonium bromide benzoic acid with 54, 64, 74, 84 units, respectively at 30 °C. The high value of the adsorption equilibrium constant reflects the high adsorption ability of this inhibitor on carbon steel surface.

From results, ΔG_{ads} values are calculated and found to be -40.40, -40.87 ,-41.43 and -42.15 kJ mol^{-1} for ethoxylted N,N,N,N-dodecyldimethyl-ammonium bromide benzoic acid with 54, 64, 74, 84 units, respectively at 30 °C. The negative values of ΔG_{ads} indicate spontaneous adsorption of the prepared surfactants on the carbon steel surface and also the strong interaction between inhibitor molecules and metal surface. Values for the

free energy of adsorption ΔG_{ads}, up to -20 kJ mol^{-1} are generally consistent with the strength of electrostatic interaction between charged molecules and charged metal (physical adsorption) while those more negative than -40 kJ mol^{-1} involve charge sharing or its transfer from the inhibitor molecules to the metal surface forming co-ordinate type of bond (chemisorption) [72].

The results obtained from **Table (22)** suggest that, the inhibitors retard the acid dissolution of steel by adsorption at steel/acid solution interface. The adsorption takes place via lone-pair and exchange mechanism by their ethylene oxide groups, while their hydrophobic chains are oriented towards the aqueous media [126]. The protection efficiencies of these inhibitors decrease in the order:

$$84 > 74 > 64 > 54$$

This is due to the different chain lengths. The increase in the length of the hydrocarbon chain causes an increase in the area of the groups attached to the adsorption center and hence reduces the rate of corrosion [127]. The data reveal that the corrosion protection efficiency decreases with an increase in temperature. This is due to decrease in the strength of adsorption process at higher temperatures, suggesting that physical adsorption of the inhibitor on the sample surfaces.

Data of **Table (22)** shows that, the values of K_{ads} are relatively large indicating that the interaction between the adsorbed molecules and the metal surface is strong physically or chemically adsorbed. The values of $K_{ads.}$ are increase with increasing the number of ethylene oxide unit and decrease with increasing temperature [128].

Analyzing the free energy of micellization data, one can get that; micellization process is spontaneous ($-\Delta G_{mic}$). Also, $-\Delta G_{mic}$ increases with increasing the number of ethylene oxide chains. This indicates that increasing of ethylene oxide chain length favors micellization process by

considering the structure of polyoxyethylene chain is favorable to hydration.

Analyzing the thermodynamic parameters of adsorption, the ΔG_{ads} values are more negative than ΔG_{mic} indicating that, the adsorption at the interface is associated with a decrease in the free energy of the system. This due to the effect of steric factor on inhibition of micellization more than its effect on adsorption.

When, ln K_{ads} is plotted against 1/T at different concentrations of the prepared surfactant as shown in **Fig. (66)**, the slope of the straight line of this curve gives the value of $-\Delta H_{ads}/R$. ΔH_{ads} values are calculated and found to be −20.80, −23.94, −28.24 and 29.90 kJ mol^{-1} for ethoxylted N,N,N,N-dodecyldimethylammonium bromide benzoic acid inhibitors with 54, 64, 74 and 84 units, respectively. The negative sign of ΔH_{ads} indicates that the adsorption of the prepared surfactants on the carbon steel surface in 1M HCl solution is an exothermic process. From results, ΔS_{ads} values are found to be 64.71, 55.85, 43.52 and 40.43 J mol^{-1} K^{-1} for ethoxylted N,N,N,N-dodecyldimethylammonium bromide benzoic acid inhibitors with 54, 64, 74, 84 units, respectively at 30 °C. The positive value of ΔS_{ads} is attributed to the increase of disorder due to the adsorption of only one surfactant molecule by desorption of more water molecules.

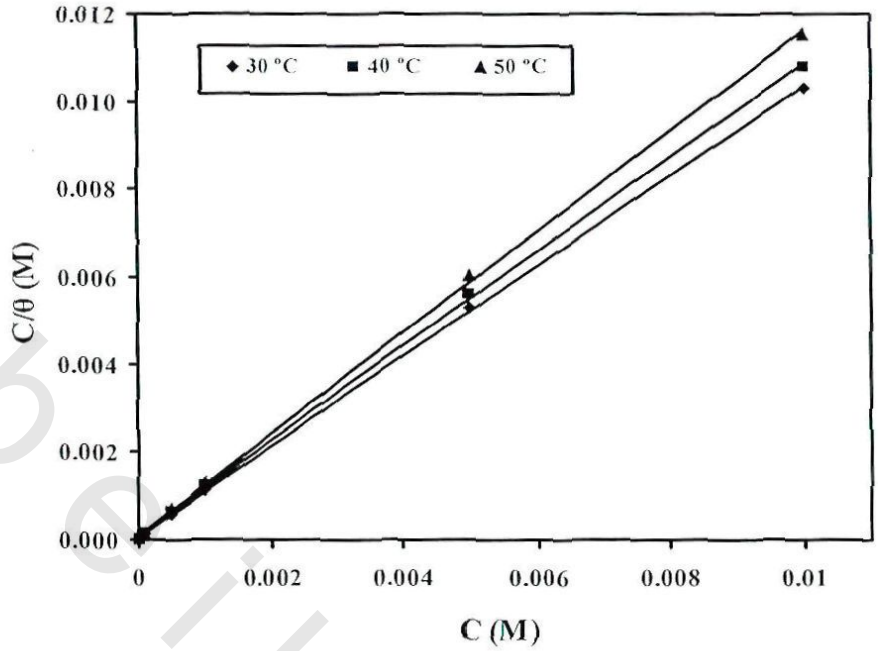

Fig. (54): Langmuir adsorption plots for carbon steel in 1M HCl in presence of different concentrations of DEDIABr at various temperatures.

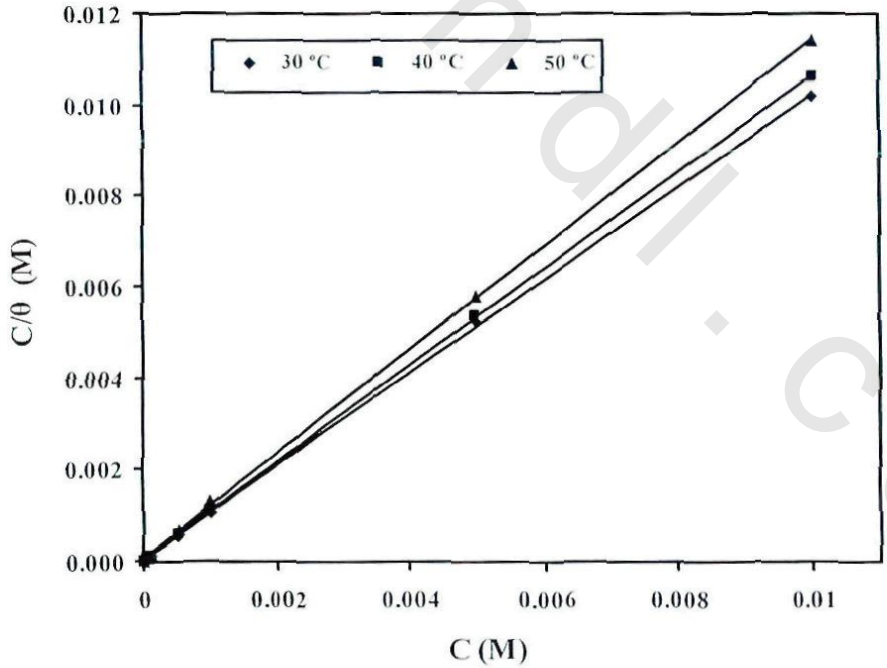

Fig. (55): Langmuir adsorption plots for carbon steel in 1M HCl in presence of different concentrations of DODIABr at various temperatures.

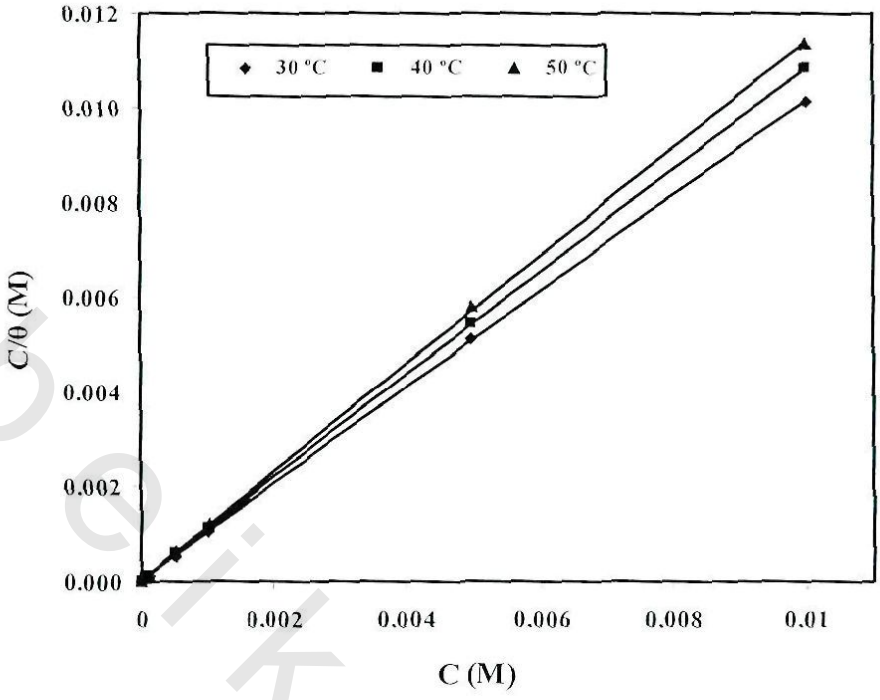

Fig. (56): Langmuir adsorption plots for carbon steel in 1M HCl in presence of different concentrations of HEDIABr at various temperatures.

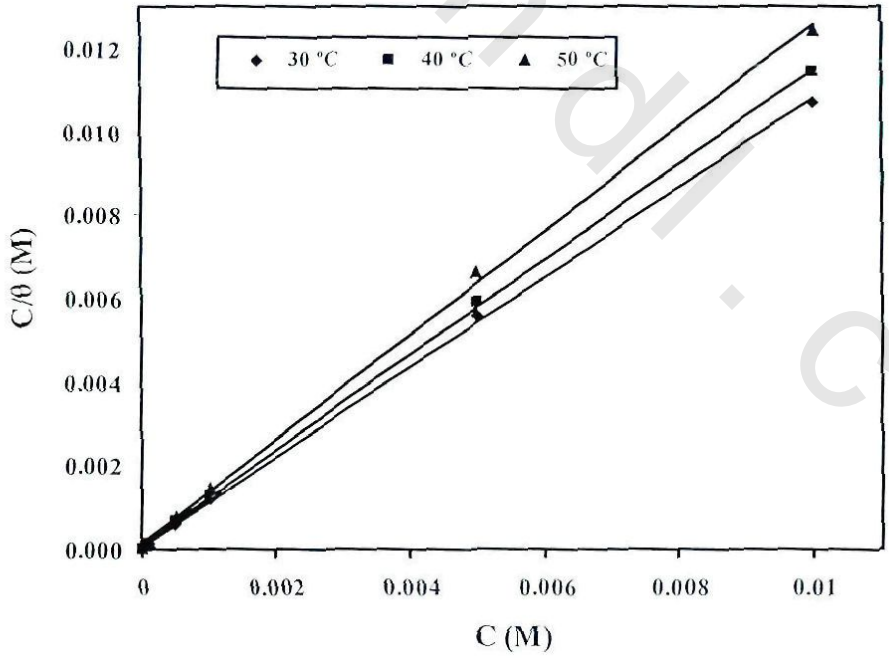

Fig. (57): Langmuir adsorption plots for carbon steel in 1M HCl in presence of different concentrations of DEDIAOH at various temperatures.

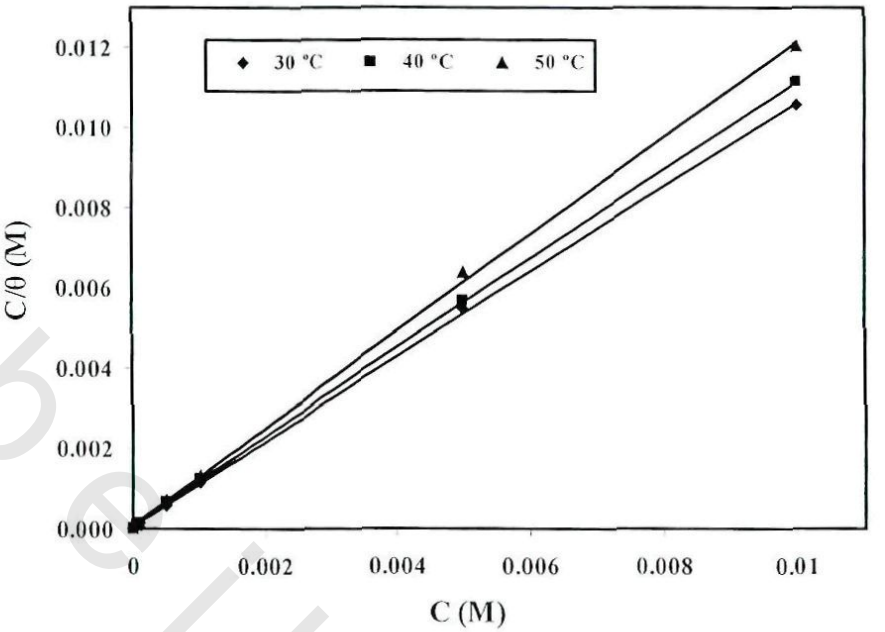

Fig. (58): Langmuir adsorption plots for carbon steel in 1M HCl in presence of different concentrations of DODIAOH at various temperatures.

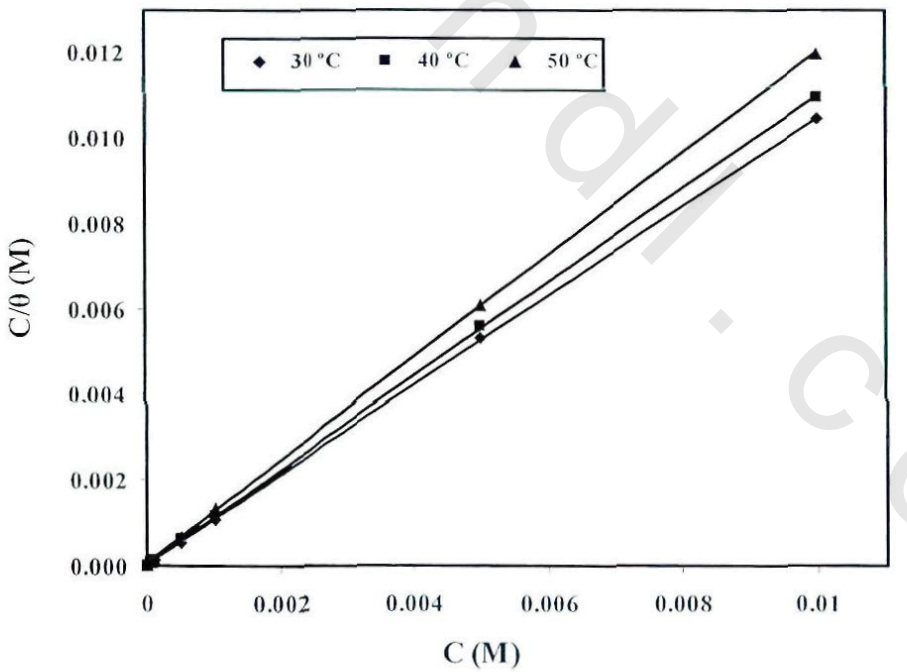

Fig. (59): Langmuir adsorption plots for carbon steel in 1M HCl in presence of different concentrations of HEDIAOH at various temperatures.

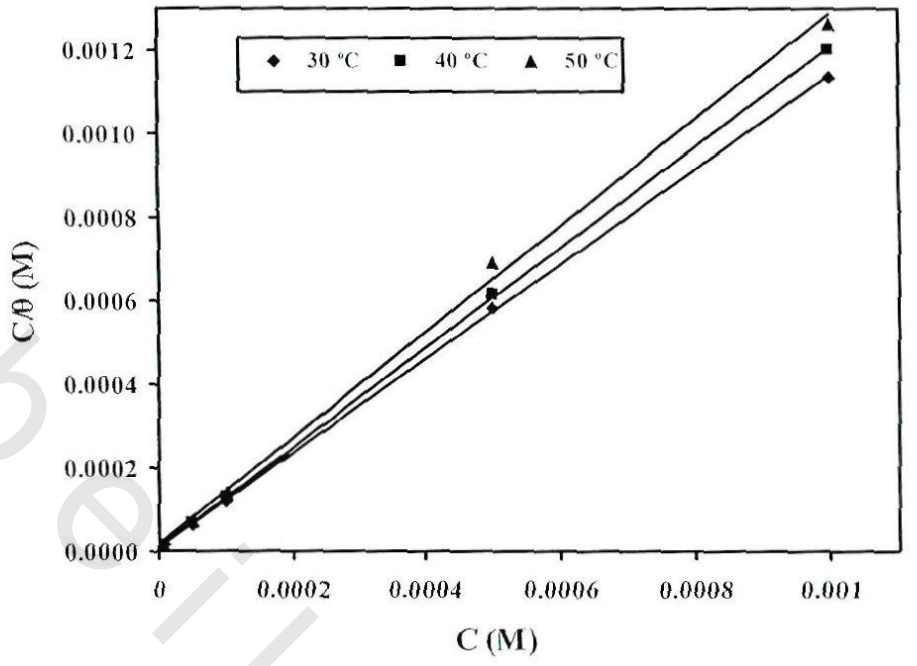

Fig. (60): Langmuir adsorption plots for carbon steel in 1M HCl in presence of different concentrations of E(54) at various temperatures.

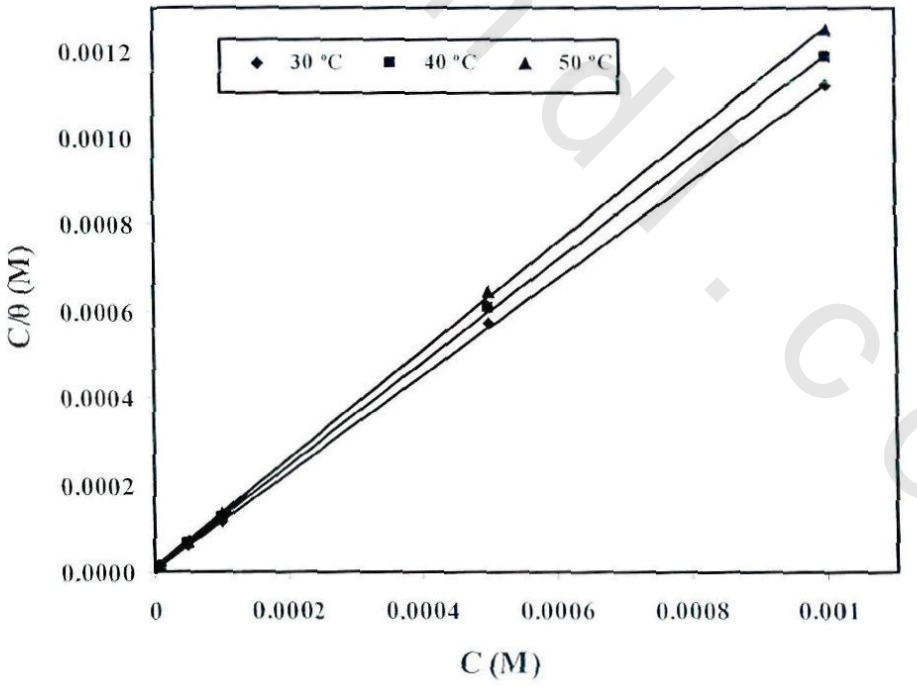

Fig. (61): Langmuir adsorption plots for carbon steel in 1M HCl in presence of different concentrations of E(64) at various temperatures.

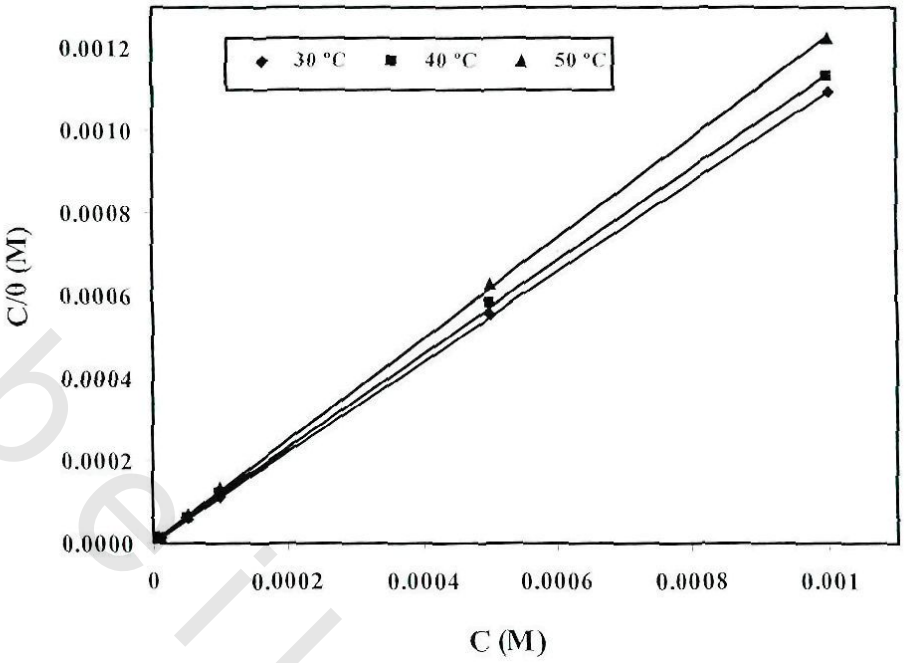

Fig. (62): Langmuir adsorption plots for carbon steel in 1M HCl in presence of different concentrations of E(74) at various temperatures.

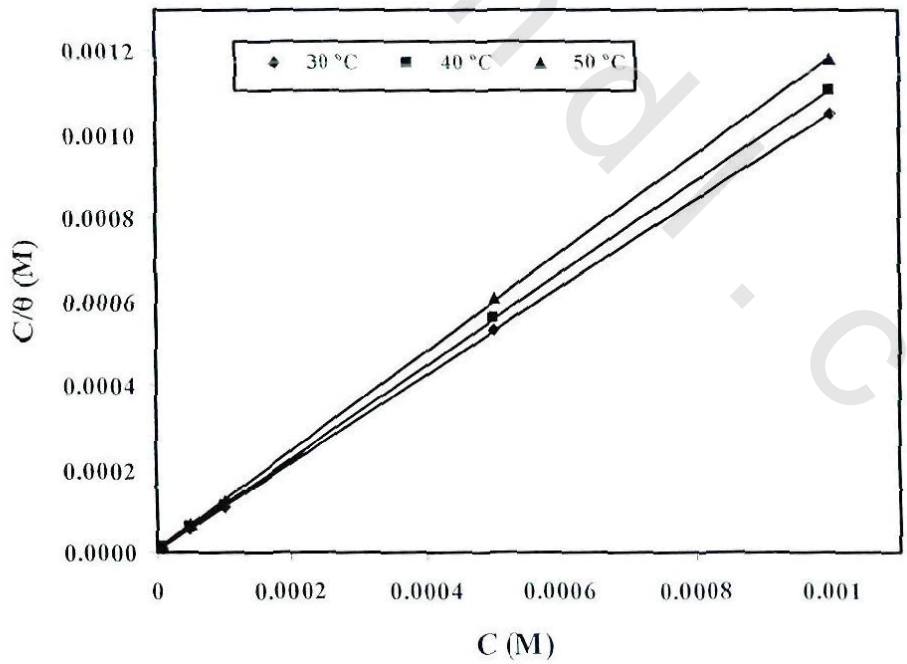

Fig. (63): Langmuir adsorption plots for carbon steel in 1M HCl in presence of different concentrations of E(84) at various temperatures.

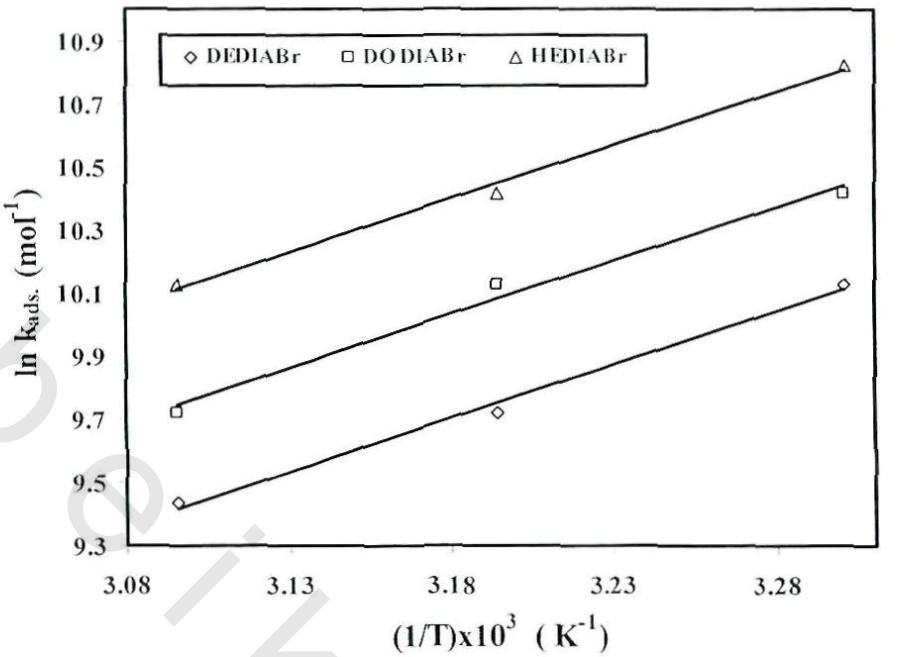

Fig. (64): Plotting of ln K_{ads} vs. (1/T) of synthesized N,N,N,N-alkyldimethyl-isopropylammonium bromide for carbon steel sample in 1M HCl at 30, 40 and 50 °C.

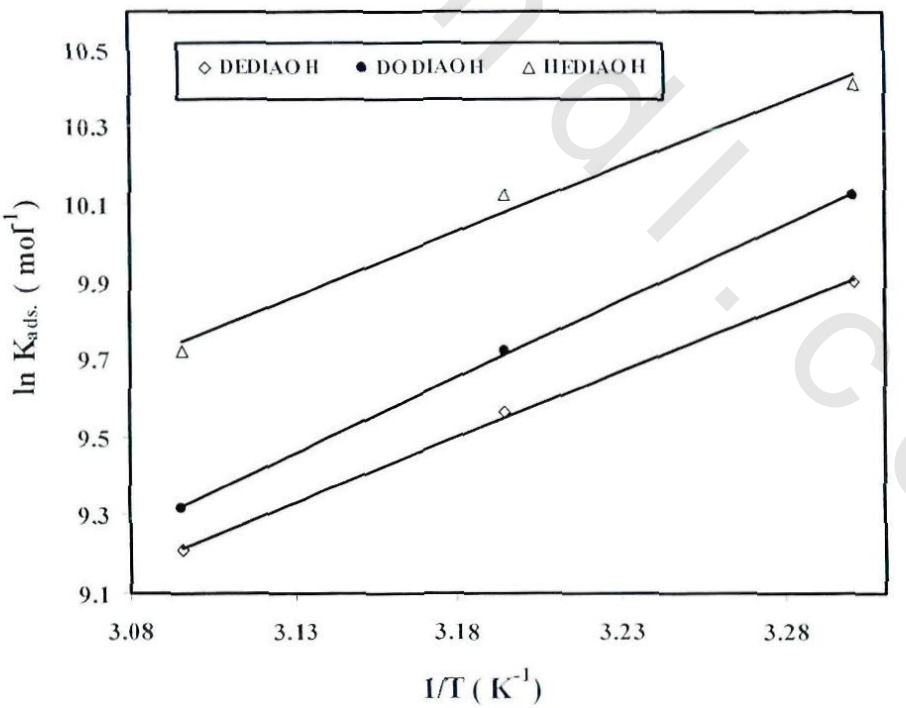

Fig. (65): Plotting ln K_{ads} vs. (1/T) of synthesized N,N,N,N-alkyldimethyl-isopropylammonium hydroxide for carbon steel sample in 1M HCl at 30, 40 and 50 °C.

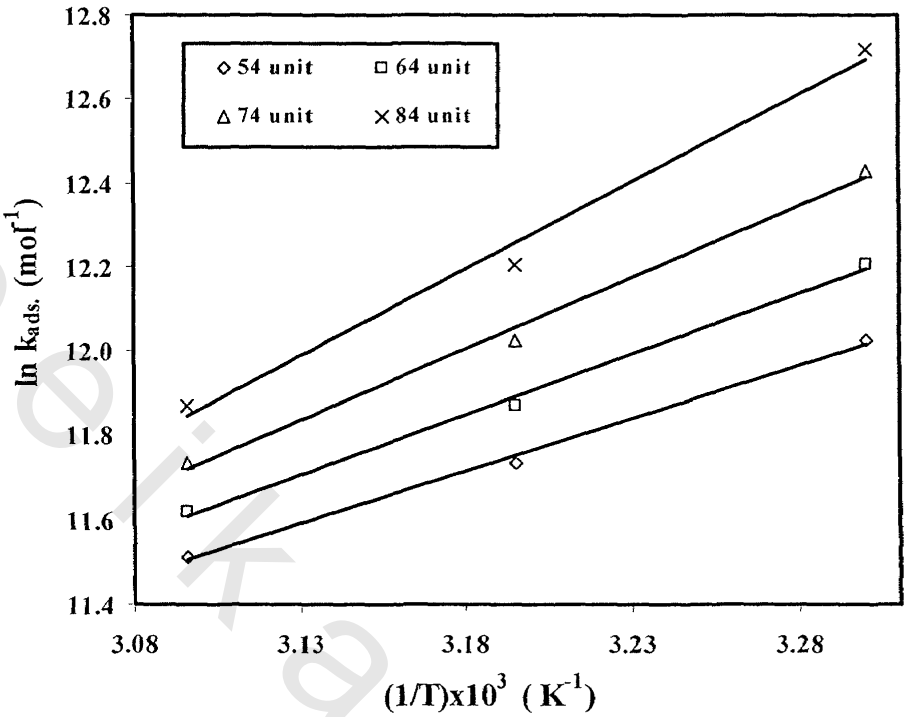

Fig. (66): Plotting ln K_{ads} vs. (1/T) of synthesized ethoxylated N,N,N,N-dodecyldimethylammonium bromide benzoic acid with 54, 64, 74, 84 units for carbon steel sample in 1M HCl at 30, 40 and 50 °C.

Table (21): The equilibrium constant and thermodynamic parameters for adsorption desorption process on carbon steel in 1M HCl containing different concentrations of synthesized cationic surfactants

Inhibitor name	Temperature °C	$K_{ads.} \times 10^4$ M^{-1}	$\Delta G_{ads.}$ kJ mol^{-1}	$\Delta H_{ads.}$ kJ mol^{-1}	$\Delta S_{ads.}$ J mol^{-1} K^{-1}
DEDIABr	30	2.50	-35.63	-28.24	24.38
	40	1.67	-35.75		23.98
	50	1.25	-36.12		24.39
DODIABr	30	3.33	-36.29	-28.09	27.06
	40	2.50	-36.74		27.64
	50	1.66	-36.83		27.05
HEDIABr	30	5.00	-37.31	-28.19	30.09
	40	3.33	-37.49		29.70
	50	2.50	-37.91		30.10
DEDIAOH	30	2.00	-35.07	-28.18	22.72
	40	1.43	-35.35		22.89
	50	1.00	-35.52		22.72
DODIAOH	30	2.50	-35.63	-32.98	8.737
	40	1.67	-35.75		8.844
	50	1.11	-35.80		8.735
HEDIAOH	30	3.33	-36.29	-28.09	27.06
	40	2.50	-36.74		27.64
	50	1.67	-36.83		27.05

Table (22): The equilibrium constant and thermodynamic parameters for adsorption desorption process on carbon steel in 1M HCl containing different concentrations of the synthesized ethoxylated N,N,N,N-dodecyldimethylammonium bromide benzoic acid.

Inhibitor name	Temperature °C	$K_{ads.} \times 10^5$ M^{-1}	$\Delta G_{ads.}$ kJ mol^{-1}	$\Delta H_{ads.}$ kJ mol^{-1}	$\Delta S_{ads.}$ J mol^{-1} K^{-1}
E(54)	30	1.67	-40.41	-20.80	64.71
	40	1.25	-40.99		64.51
	50	1.00	-41.70		64.70
E(64)	30	2.00	-40.87	-23.94	55.85
	40	1.43	-41.34		55.58
	50	1.11	-41.99		55.86
E(74)	30	2.50	-41.43	-28.24	43.52
	40	1.67	-41.74		43.13
	50	1.25	-42.30		43.53
E(84)	30	3.33	-42.15	-29.90	40.43
	40	2.00	-42.22		39.33
	50	1.43	-42.66		39.49

2.10. Scanning electron microscopy (SEM) of surfactants

SEM image of steel surface specimen after immersion in 1M HCl solution for 24 h are shown in **Figs. (67a-69a)**. The micrograph reveals that, the surface is strongly damaged in absence of inhibitors. SEM image of another steel surface specimen after immersion for the same time interval in 1M HCl solution containing $1x10^{-2}$ M of DEDIABr, DODIABr and HEDIABr, respectively are shown in **Figs. (67b-67d)**, SEM image for DEDIAOH, DODIAOH and HEDIAOH, respectively are shown in **Figs. (68b-68d)** and SEM image for ethoxylated-cationic surfactant inhibitors with 54, 64, 74, 84 units, respectively are shown in **Figs. (69b-69f)**. The micrographs reveal that, the surface in presence of inhibitors is free from pits and it is smooth which indicates formation of a good protective film present on the steel surface and also confirms the highest inhibition efficiency of the prepared surfactants at $1x10^{-2}$ M concentration.

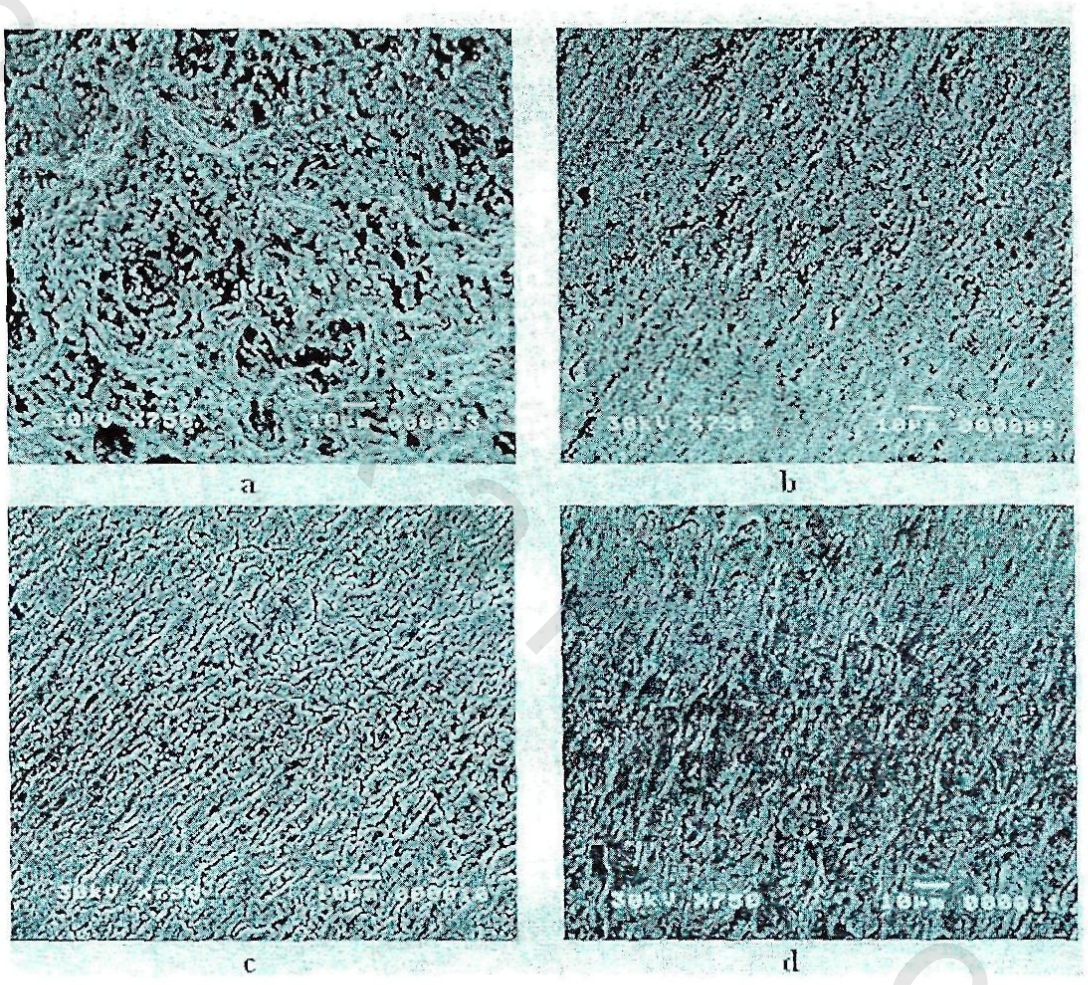

Fig. (67): *SEM image of surface of carbon steel after immersion for 24 h at 30°C in 1M HCl (a) and in presence of 1 x 10^{-2} M from each of DEDIABr (b), DODIABr (c) and HEDIABr (d). Magnification X750.*

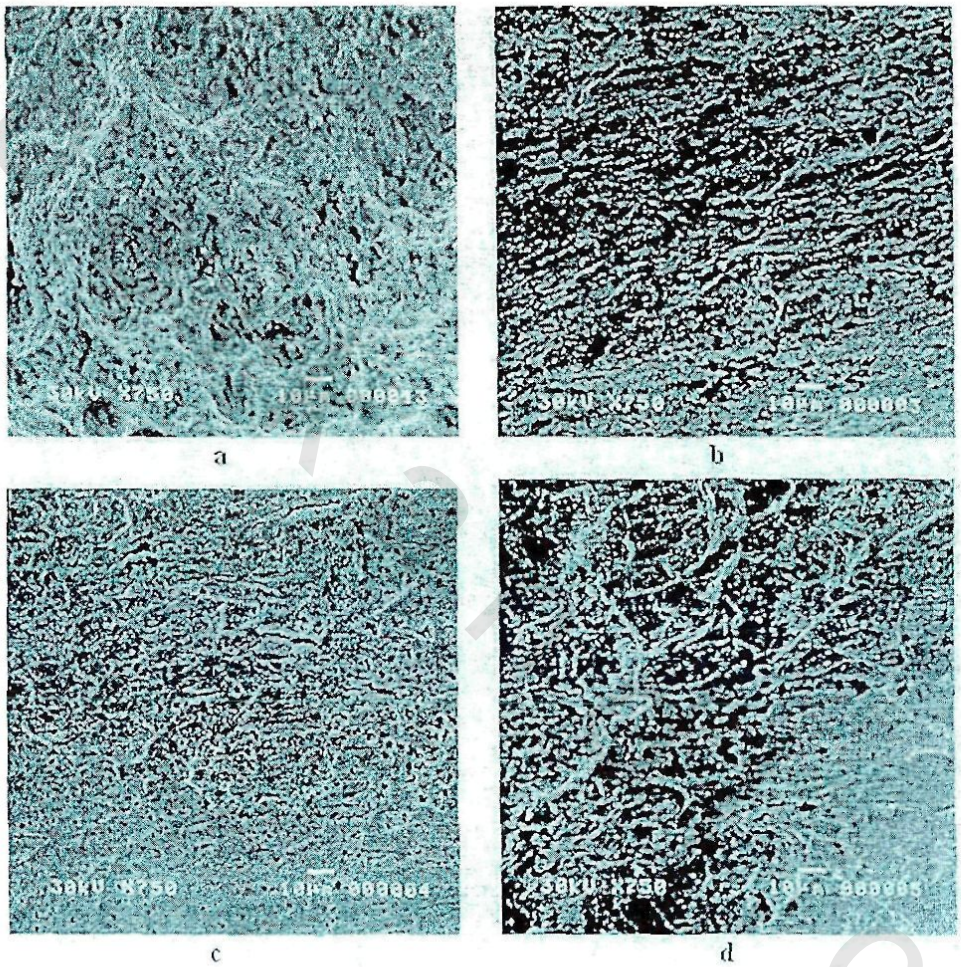

Fig. (68): SEM image of surface of carbon steel after immersion for 24 h at 30°C in 1M HCl (a) and in presence of 1 x 10^{-2} M from each of DEDIAOH (b), DODIAOH (c) and HEDIAOH (d). Magnification X750.

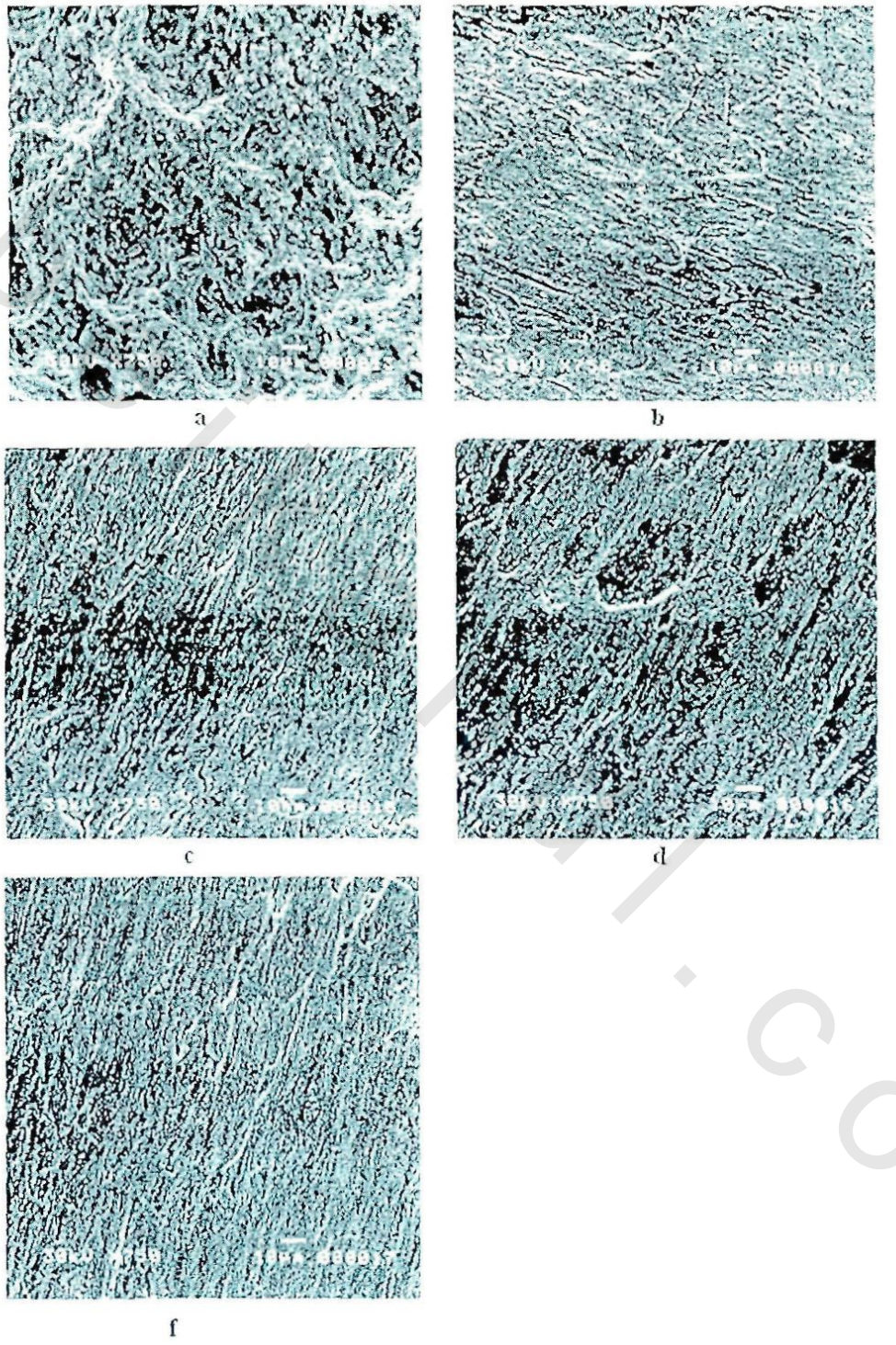

Fig. (69): SEM image of surface of carbon steel after immersion for 24 h at 30°C in 1M HCl (a) and in presence of 1 x 10^{-2} M from each of E(54) (b), E(64) (c), E(74) (d) and E(84) (f). Magnification X750.

2.11. Antimicrobial activity of the prepared surfactants against sulfate reducing bacteria (SRB)

Generally, biocides exert their bacteriostatic effect on sensitive organisms by:

1. Inhibition cell wall permeability.
2. Injuring the cytoplasmic membrane.
3. Inhibition the protein biosynthesis.
4. Inhibition the nucleic acid synthesis.

The results of antimicrobial activity of synthesized cationic surfactant biocides against SRB were determined by dilution method and listed in **Table (23)**. The results indicate that the synthesized cationic surfactants have antimicrobial activity against the tested microorganisms (SRB) and their activities depend on their chemical structures (mainly the hydrophobic chain length). The optimal potency of the synthesized corrosion inhibitors was observed on the dodecyl chain (12-methylene groups). These results are in good agreements with the results of several investigators who dealt with the cationic biocides [129-133]. The action mode of such cationic biocides on the bacterial strain is explained as an electrostatic interaction and physical disruption. The electrostatic interaction occurs between the oppositely charged centers on the cellular membrane and the positively charged head groups of the biocide molecules. While, physical disruption results are from the penetration of the hydrophobic chains into the cellular membrane due to the similarity in the chemical nature. The interaction between biocide molecules and cellular membrane causes, a strong damage of the selective permeability of these membranes which disturbs the metabolic pathway within the cytoplasm [134].

The results indicate that, the synthesized ethoxylated-cationic surfactants showed weak antimicrobial activity against the tested microorganisms (SRB).

Table (23): Antimicrobial activity of synthesized surfactants against sulfate reducing bacteria by dilution method.

Inhibitor name	Bacteria count (Colony/ml sample) (*Desulfomonas pigra*)					
	Control	**10^{-5}**	**10^{-4}**	**10^{-3}**	**10^{-2}**	**10^{-1}**
DEDIABr	$7.23x10^3$	$6.88x10^3$	$6.13x10^3$	$4.92x10^3$	786	0.0
DODIABr	$7.13x10^3$	$6.21x10^3$	$4.29x10^3$	216	0.0	0.0
HEDIABr	$6.88x10^3$	$5.95x10^3$	$4.12x10^3$	640	0.0	0.0
DEDIAOH	$6.94x10^3$	$6.29x10^3$	$5.89x10^3$	$3.72x10^3$	0.0	0.0
DODIAOH	$7.28x10^3$	$6.30x10^3$	$2.68x10^3$	6.00	0.0	0.0
HEDIAOH	$6.36x10^3$	$6.19x10^3$	$5.97x10^3$	$4.82x10^3$	620	0.0
E(54)	$6.82x10^3$	$6.89x10^3$	$6.63\ x10^3$	$6.17\ x10^3$	$5.93\ x10^3$	$5.42\ x10^3$
E(64)	$6.82x10^3$	$6.93\ x10^3$	$6.69\ x10^3$	$6.52\ x10^3$	$2.28\ x10^3$	$0.66\ x10^3$
E(74)	$6.82x10^3$	$6.36\ x10^3$	$6.21\ x10^3$	$5.98\ x10^3$	$3.21\ x10^3$	$1.96\ x10^3$
E(84)	$6.82x10^3$	$6.78\ x10^3$	$6.33\ x10^3$	$5.19\ x10^3$	$4.81\ x10^3$	$3.31\ x10^3$